QUANTITATIVE ULTRASOUND: LOW VARIANCE ESTIMATION OF BACKSCATTERING AND ATTENUATION COEFFICIENTS

ZARA VAJIHI

A THESIS

IN

THE DEPARTMENT

OF

ELECTRICAL AND COMPUTER ENGINEERING

PRESENTED IN PARTIAL FULFILLMENT OF THE REQUIREMENTS

FOR THE DEGREE OF MASTER OF APPLIED SCIENCE

CONCORDIA UNIVERSITY

MONTRÉAL, QUÉBEC, CANADA

NOVEMBER 2018

CONCORDIA UNIVERSITY

School of Graduate Studies

This is to certify that the thesis prepared

By: **Zara Vajihi**

Entitled: **Quantitative ultrasound: low variance estimation of backscattering and attenuation coefficients**

and submitted in partial fulfillment of the requirements for the degree of

Master of Applied Science

complies with the regulations of this University and meets the accepted standards with respect to originality and quality.

Signed by the final examining commitee:

_____ Chair
Dr. Wahab Hamou-Lhadj

_____ External Examiner
Dr. Tiberiu Popa

_____ Examiner
Dr. Wahab Hamou-Lhadj

_____ Supervisor
Dr. Hassan Rivaz

Approved by: _____
Dr. W. E. Lynch, Chair
Department of Electrical and Computer Engineering

_____ 20 _____ _____

Dr. Amir Asif, Dean

Gina Cody School of Engineering and Computer Science

Abstract

Quantitative ultrasound: low variance estimation of backscattering and attenuation coefficients

Zara Vajihi

One of the main limitations of ultrasound imaging is that image quality and interpretation depend on the skill of the user and the experience of the clinician. Quantitative ultrasound (QUS) methods provide objective, system-independent estimates of tissue properties such as acoustic attenuation and backscattering properties of tissue, which are valuable as objective tools for both diagnosis and intervention. Accurate and precise estimation of these properties requires correct compensation for intervening tissue attenuation. Prior attempts to estimate intervening-tissues attenuation based on minimizing cost functions that compared backscattered echo data to models have resulted in limited precision and accuracy. The first contribution of this thesis is that we incorporate the prior information of piecewise continuity of QUS parameters as an L2 norm regularization term into our cost function to overcome these limitations. We further propose to calculate this cost function using Dynamic Programming (DP), a computationally efficient optimization algorithm that finds the global optimum. Our results on tissue-mimicking phantoms show that DP substantially outperforms a state-of-the-art method in terms of both estimation bias and variance.

The second contribution of this thesis is that to further improve the accuracy and precision of this DP method, we propose to use L1 norm instead of L2 norm as the regularization term in our cost function and optimize the function using DP. Our results show that DP with

L1 regularization reduces bias of attenuation and backscatter parameters even further compared to DP with L2 norm. Besides, we employ DP to estimate the QUS parameters of a new phantom with large scatterer size and compare the results of LSq, L2 norm DP and L1 norm DP. Our results show that L1 norm DP outperforms L2 norm DP, which itself outperforms LSq. In the future, the contributions of this thesis can potentially be used for finding imaging biomarkers associated with different types of pathology and help clinicians obtain an objective assessment of intrinsic tissue properties.

Acknowledgments

I would like to extend my thanks to many people who so kindly contributed and supported the work presented in this thesis.

Special appreciation goes to my enthusiastic supervisor, Dr. Rivaz, who continuously believed and supported me in every step of my research. My Masters has been an amazing experience and I thank him for steering me toward the summit.

Similarly, profound gratitude goes to Dr. Mendez and Dr. Hall for their constant guidance and valuable inputs. I am honored to have the chance to perform this study with their collaboration.

Also, I would like to express my thanks to all the nice researchers, staff and fellow students at PERFORM center for the gracious and peaceful atmosphere. All the discussions, laughs, and warmth shared during the coffee breaks and meals made me feel being at home and working with my beloved family.

Last, but by no means least, greatest thanks go to my parents, two angles in my life who had taught me how to live a true human being and spread love and passion to the universe. I love them and will be indebted to them forever.

This work was partly supported by Natural Science and Engineering Research Council of Canada (NSERC) Discovery grant RGPIN-2015-04136.

Contents

List of Figures

List of Tables

Chapter 1

Introduction

In this chapter, the fundamental aspects of Ultrasound imaging are studied. A brief history of ultrasound utilization is given at the beginning. Then, the physics of ultrasound is explained and some of the applications of it are reviewed. Finally, an overview of quantitative ultrasound which is the main concentration of this thesis is provided.

1.1 Basic Physics of Ultrasound

Ultrasound waves were initially used in submarines in the early 19th century for navigation. It was initiated to the medical field about 50 years later for diagnosis and treatment purposes. With the technological advancements in electronics and computation, ultrasound machines developed to a worldwide imaging technique with a variety of applications [1].

Ultrasound or Ultrasonic (US) waves are sound waves with a frequency of higher than 20 kHz, which exceed the upper limit of audible sounds for human hearing [2]. US is categorized as mechanical waves with longitudinal motion, i.e. it moves along the substances by compression and expansion without any side-to-side movement [3].

Ultrasound machines utilize ultrasound waves in the typical frequency range of 1 to

Figure 1: A Supersonic Imagine ultrasound machine at PERFORM center

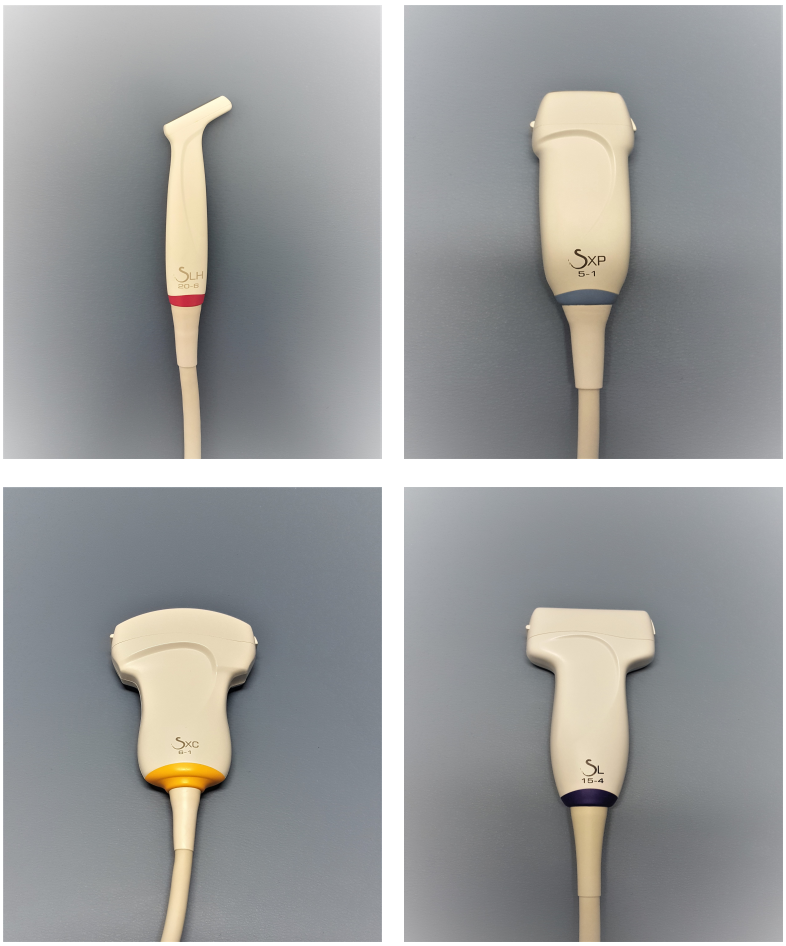

Figure 2: Four different ultrasound transducers available at PERFORM center

20 MHz to inquire information about the human organs. These waves are beamed to the region of interest of the human body using a device named transducer (or probe). The transducer is an electronic device consisting of multiple piezoelectric crystals [4, 5]. Based on the different arrangements of the piezoelectric crystals and consequently, their different applications, a variety of US transducers are available in the market. Fig. 1 is a picture of one of the available US machines for the research purpose at PERFORM center. Fig. 2 represents four different transducers of this machine.

The transducer, first, converts the electrical charge into vibrations, which produce ultrasound waves. This phenomenon is named as the piezoelectric effect, which was originally

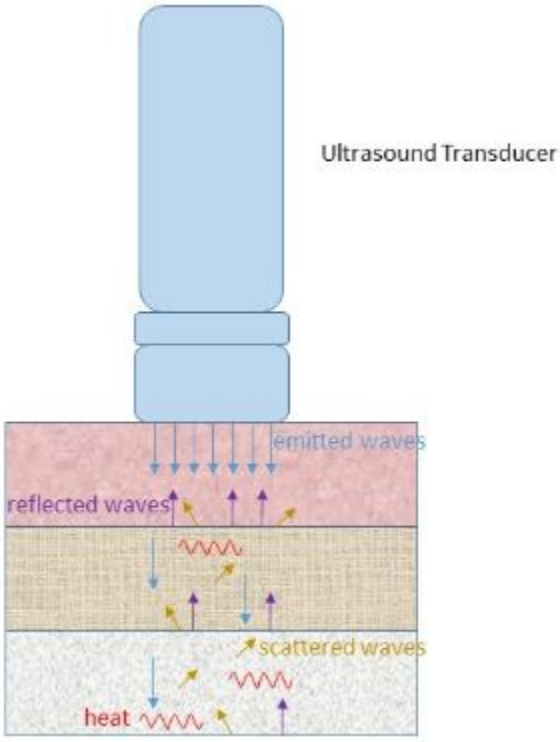

Figure 3: Ultrasound wave interactions with tissue

introduced in 1880. The US waves penetrate the human body and travel through different tissue layers with various acoustic characteristics along the transmission path (Fig. 3). A small fraction of US waves reflect back to the transducer from the boundaries of layers, whereas the remainder continues penetrating deeper, dissipate in form of heat, or scatter in other directions. The reflected echoes are received by the transducer and converted to electrical pulses for further process. These received pulses are technically called Radio Frequency (RF) data.

Similar to any other sound wave, reflected US waves can be described in terms of frequency, wavelength, and amplitude which are respectively measured in Hertz, millimeter, and decibel. Each of these parameters carries important information about the properties of scanned tissue and can be interpreted for different purposes.

The primary interpretation of US waves is constructed from the amplitude of the wave

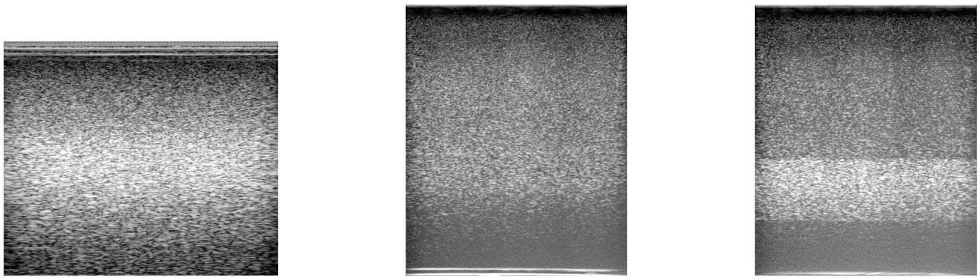

(a) Uniform Phantom (b) Layered Phantom with Uniform Backscatter (c) Layered Phantom with Uniform Attenuation

Figure 4: B-mode image of three different tissue-mimicking phantoms

at different time delays. The gray-scale image displayed on the clinical US machine screen, called B-mode image, is basically the envelope detection of the reflected US wave. In the B-mode image, organs with different density are represented with a different brightness which is due to different acoustic impedances. Acoustic impedance is defined as the multiplication of density parameter by the velocity of the wave in the tissue [6, 7]. The B-mode image of three phantoms that were used in this work is represented in Fig. 4.

Generally, organs that contain air, such as lungs, have lowest acoustic impedance, while dense organs, like bones, have the highest acoustic impedance. This variety in acoustic impedance of human organs results in proportional reflection of echoes and consequently, different brightness in the B-mode image. Nevertheless, it requires deep knowledge of human anatomy and vast experience in using US images for a radiologist or practitioner to be able to correctly employ the reproduced B-mode images to diagnose any irregularity in patient's body.

Moreover, within a uniform tissue, there are normally some particles causing partial scatterings that lead to a rise in the scattering of any sub-resolution structures [8]. These partial scatterings appear as speckles in B-Mode images that could make the analysis of the US images more difficult. Many research and efforts have been done on reducing these

scatterings effects and make the B-mode images more distinct. However, these particles actually define microstructure of the material.

Therefore, carefully studying the signals that are reflected back from these speckles lead us to a more accurate understanding of the tissue characteristics. Tracking these speckles in the images collected before and after compression of the tissue reveals the stiffness of it at the different depth which is called elastography [9, 10]. Analyzing the speckles in US images are also used for the purpose of segmentation, sensorless 3D freehand US, and tissue type classification [11, 12, 13].

1.2 Quantitative Ultrasound

As mentioned before, the ultrasound B-mode image represents a qualitative map of human body tissue so that the radiologist or practitioner can detect any strangeness in the tissue such as a tumor. However, it is not easy, and not even possible in many cases, to realize the type of irregularity or the tumor by investigating the B-mode image. Regularly, a biopsy is required to find out the quantitative specifications of the tumor and diagnosing it as a benign or malignant cancer which leads to different treatment procedures.

Despite all the risks, costs, and difficulties of biopsy, a large group of them results in a negative result which means it was not necessary to perform the biopsy. Even for those positive results, there is a high risk of spreading or infection for existing cancer. Therefore, it is highly desired to have a safer and less destructive solution to find out the quantitative properties of the abnormal tissue. Quantitative Ultrasound, which is the subject of this thesis, is one of the most successful and easily applicable solutions for this problem [14].

Quantitative Ultrasound (QUS) studies the RF data collected to find out the backscattering and attenuation properties of the US wave reflected from the tissue [15]. These two specifications are different for various types of the tissue and could specifically determine

the class of any tumor or cyst. Being non-invasive and widely available, QUS could be a valuable substitution for harmful methods like the biopsy [16].

There have been many studies in QUS that suggest different analysis of RF data to find either backscattering or the attenuation of the tissue and various applications for them [17, 18, 19]. However, the proposed methods have not yet provided the adequate accuracy required to be used in clinical applications. In this thesis, a research in QUS field is conducted to find a better method in estimating microstructure properties of tissues.

1.3 Thesis Outline

In Chapter 2, a novel method is introduced for estimating the backscatter and attenuation properties of tissue using a dynamic programming approach. Dynamic programming globally searches over all possible solutions and finds the optima [20]. Moreover, an L2 norm regularization term is added to the cost function which resulted in a low variance estimation for unknowns. Finally, the results of this novel method were compared to the results of a previous state-of-the-art work [21]. It is clearly shown that this method successfully provides more accurate and precise estimations for quantitative coefficients of tissue. This work is published as a journal paper in IEEE Transactions on Ultrasonics, Ferroelectrics, and Frequency Control (IEEE TUFFC).

In Chapter 3, both the novel method proposed in Chapter 2 and the previous work by Kibo et al. [21] were applied to the data acquired from a tissue mimicking phantom with large scatterer size. Despite the difficulty of estimation with the presence of large scatterers, the proposed method succeeds to provide a highly accurate estimation for the unknown values. Finally, the substitution of L1 norm is suggested for the regularization in Chapter 3 to have a more accurate estimation in discontinuities of unknown values. The results of this chapter are submitted as a conference paper to the IEEE International Symposium on

Biomedical Imaging (ISBI), 2019, which is currently under revision.

Chapter 2

Low Variance Estimation of Backscatter Quantitative Ultrasound Parameters Using Dynamic Programming

This chapter is published in IEEE Transactions on Ultrasonics, Ferroelectrics, and Frequency Control [22].

2.1 Introduction

Ultrasound is an inexpensive, real-time, safe and easy-to-use imaging modality that is widely used in numerous clinical applications. However, it only provides qualitative brightness values, which cannot be directly used for classification of tissue pathology. Quantitative ultrasound (QUS) aims to solve this limitation by providing attenuation and backscattering properties of the tissue. As such, QUS has numerous applications in both diagnosis and therapy monitoring. Some clinical applications of attenuation estimation include differentiation of fatty liver from normal liver [23], monitoring of liver ablation [24], diagnosis

of thyroid cancer [25, 26] and assessment of bone health [27, 28, 29]. Backscatter estimation has been successfully used in the classification of benign versus malignant masses in several different organs such as eyes [30], breast [31, 32, 33] and thyroid [34, 35], and used to monitor the normal function of kidneys [36]. A review of recent QUS techniques and applications can be found in [37, 38].

Nevertheless, QUS has been less widely translated into clinical applications compared to ultrasound elastography. This is mainly due to the difficulty in accurately and precisely estimating attenuation and backscattering. To address this issue, Nam et al. [21] proposed a Least Squares (LSq) method to simultaneously estimate backscatter and attenuation coefficients. Although this method substantially improved the results compared to the commonly used Reference Phantom Method (RPM) [39], it calculates these parameters at each spatial location independent of its neighbors and hence neglects spatial dependency of these coefficients. More recently, Coila et al. [40] adapted the conventional spectral log difference technique for attenuation estimation by adding a regularization term. Despite substantially improving the results, this work only estimates attenuation (not backscattering). These two properties are closely related and our goal is to simultaneously calculate both of them.

In this chapter, we propose a novel cost function that incorporates both data terms and spatial information in the form of regularization. We propose to use the Dynamic Programming (DP) method to optimize this cost function. DP breaks the main cost function into small problems, and efficiently obtains the global optimum by exploiting overlapping computations in these sub-problems. An analogous use of DP has been reported to estimate high-quality displacement estimates in ultrasound elastography [41, 42] and in computer vision [43].

This chapter is summarized as follows. In Section 3.2, we show how the spatial relationship of attenuation and backscatter coefficients can be incorporated into a cost function, and outline the proposed DP framework for optimization of the cost function. Experiments

and results on phantoms are provided in Section 3.4, and the chapter is concluded in Section 3.5.

2.2 Methods

Quantitative ultrasound often aims at estimating attenuation and backscatter properties of tissues, and parameters derived from them. The total attenuation along an RF line is usually modeled as:

$$A(f, z) = exp(-4\alpha f z) \tag{1}$$

where A is the total attenuation corresponding to frequency f and depth z, and α is the effective attenuation coefficient versus frequency (i.e., the average attenuation from intervening tissues). Backscatter coefficients are often parametrized with the following power law equation:

$$B(f) = bf^n \tag{2}$$

where b is a constant coefficient and n represents the frequency dependence. Our goal is to find the values of α, b and n from Eqs. 18 and 19.

The framework for the proposed algorithm is based on the Reference Phantom Method developed by Yao et al [39]. Let $S_s(f, z)$ and $S_r(f, z)$ be, respectively, the sample and reference echo signal power spectra computed from radiofrequency (RF) echo signals obtained from scanning a tissue sample (or a tissue-mimicking test phantom) and a reference phantom (of known acoustic properties) with the same ultrasound transducer and the same imaging settings (i.e. frequency, focal properties, etc). Taking the ratio of the two spectra eliminates any dependence on the imaging setting (assuming the media have equivalent

sound speeds [44]), leaving only attenuation and backscatter-dependent terms:

$$RS(f,z) = \frac{S_s(f,z)}{S_r(f,z)} = \frac{B_s(f)}{B_r(f)} . \frac{A_s(f,z)}{A_r(f,z)} = \frac{b_s f^{n_s}}{b_r f^{n_r}} exp\{-4(\alpha_s - \alpha_r) f.z\} \tag{3}$$

where the subscripts s and r refer to the sample and the reference phantom, respectively. Taking the natural logarithm of Eq. 20 leads to

$$\ln \frac{S_s(f,z)}{S_r(f,z)} = \ln \frac{b_s}{b_r} + (n_s - n_r) \ln f - 4(\alpha_s - \alpha_r) f.z. \tag{4}$$

Substituting the following variables:

$$\ln \frac{S_s(f,z)}{S_r(f,z)} \equiv X(f,z), \;\; \ln \frac{b_s}{b_r} \equiv b, \;\; n_s - n_r \equiv n, \;\; \alpha_s - \alpha_r \equiv \alpha \tag{5}$$

into Eq. 4 leads to:

$$X(f,z) = b + n \ln f - 4\alpha f z \tag{6}$$

where X is known from the experimental data, and the goal is to estimate α, b and n, which reveal quantitative properties of the sample.

In the next section, we first briefly overview the Least Squares (LSq) method for recovering these parameters [21]. We will then present a novel framework wherein continuity of quantitative tissue properties is incorporated into the cost function. We also propose a global, yet efficient, optimization of this cost function using DP.

2.2.1 Least Squares (LSq) Method

Nam et al. [21] proposed the following LSq formulation for estimating α, b and n:

$$[\hat{\alpha}, \hat{b}, \hat{n}] = \arg\min_{\alpha,b,n} D \tag{7}$$

where the data term D (in contrast to a regularization term that we will introduce later in Eq. 22) is:

$$D = \sum_{i=1}^{K} (X(f_i,z) - b - n \ln f_i + 4\alpha f_i z)^2 \tag{8}$$

where the summation is over the frequency range of X. The search range for these parameters is usually confined as follows:

$$\alpha_1 \leq \alpha \leq \alpha_2, \;\; b_1 \leq b \leq b_2, \;\; n_1 \leq n \leq n_2 \tag{9}$$

where α_1 and α_2 , b_1 and b_2, and n_1 and n_2 are the lower and upper search limits for the attenuation coefficient α, the magnitude of the backscatter coefficient b, and the frequency dependence of the backscatter coefficient n, respectively. Search ranges contained $k = 1, ..., K$ discrete values for α, $l = 1, ..., L$ discrete values for b, and $m = 1, ..., M$ discrete values for n.

The aforementioned LSq formulation does not consider the fact that the properties of the sample do not arbitrarily change across the phantom, and therefore can result in estimates with large variance. The proposed Dynamic Programming (DP) framework in the next section addresses this issue.

2.2.2 Dynamic Programming (DP)

Parameters α, b and n can rapidly change from one tissue type to another, but they change gradually within each tissue type. Thus, these parameters can be considered piece-wise continuous [45]. This condition can be used to improve parameter estimation. Similar to our previous work in the field of elastography [41, 42], we proposed a regularized cost function that incorporates both data terms and prior information for parameter estimation. Our cost function has the general form of

$$C = D + wR \tag{10}$$

where D is the data term of Eq. 8, w and R are the vector of regularization weights and a regularization term, respectively, defined as:

$$w = [w_\alpha, w_b, w_n] \tag{11}$$

$$R = (\alpha_j - \alpha_{j-1})^2 + (b_j - b_{j-1})^2 + (n_j - n_{j-1})^2 \tag{12}$$

with subscripts j and $j-1$ referring to axial positions at the current and previous rows, and w_α, w_b, and w_n are the regularization weights for each unknown. Let vector $\mathbf{u}$ encapsulate the unknowns as follows:

$$\mathbf{u} = [\alpha, b, n] \tag{13}$$

To find the global minimum of this cost function, we use the efficient DP framework, and formulate the following recursive cost function:

$$C(j, \mathbf{u}_j) = \min_{\mathbf{u}} \{C(j-1, \mathbf{u}_{j-1}) + wR(\mathbf{u}_{j-1}, \mathbf{u})\} + \Delta(j, \mathbf{u}) \tag{14}$$

where $\Delta(j, \mathbf{u})$ is:

$$\Delta(j, \mathbf{u}) = \Delta(j, \alpha, b, n) = \sum_{i=1}^{K} (X(f_i, z) - b - n \ln f_i + 4\alpha f_i z)^2 \tag{15}$$

The minimization is performed on three unknowns $\mathbf{u}$ at each location. The cost function in Eq. 28 is formed as a 4D matrix C_{jklm} including the location (z_j) as well as vector $\mathbf{u}$ with components [α_k, b_l, n_m] where j refers to each of the $j = 1, ..., J$ axial positions, $k = 1, .., K$, $l = 1, ..., L$ and $m = 1, ..., M$ refer to the discrete search range values of parameters α, b, and n.

As a simplified illustrative example, Fig. 5 shows a 2D version of C_{jklm}, i.e., C_{jk} which considers only one unknown, attenuation coefficient α. We allocate a 2D matrix to store different values of C_{jk} as z_j and α_k vary (Fig. 6). Every cell in this matrix is filled with cost values at the associated α_k and depth with that cell. In order to find the cost value at a cell in Fig. 6, we first calculate the Δ term in Eq. 28 at z_j and the corresponding α_k. Then, the minimization part in Eq. 28 is performed. The index $j-1$ in this term indicates that the cost value at depth j depends on the cost value at the previous depth. In other words, we add the values stored in row z_{j-1} to the regularization term (Eq. 12) and find its minimum.

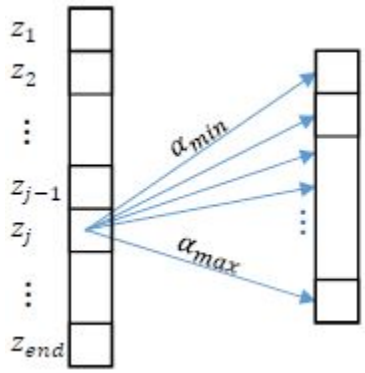

Figure 5: At each ROI z_j , different values of α_k, b_l, and n_m are explored. To simplify illustration, only α is shown in this figure.

We also store the values of unknown coefficients for which this minimization occurs (a step technically known in DP as *memoization*). These locations are stored in M, a 2D matrix with the same size as C in this reduced example. Finally, the Δ term added to the minimum value is stored as the value of the cost function at the corresponding cell to be used for the next depth.

The DP cost function must be calculated for every axial row. After that, a final minimization is performed on the cost function in the last row to estimate the α at that depth. Then, starting from the values stored in M, we trace back the minimum points to the first row using the memoization matrix M.

Extending this reduced example of DP to the quantitative ultrasound problem in Eq. 28 with three unknowns, $\mathbf{u}$, and depth dependency, the matrix in Fig. 6 as well as memoization matrix M change to 4D matrices. Consequently, cost values at depth j illustrated as a row in Fig. 6 will be a 3D matrix as shown in Fig. 7.

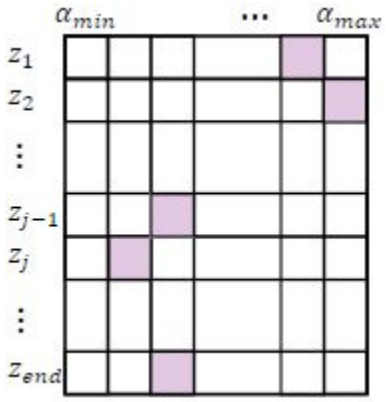

Figure 6: 2D matrix of cost values at different depths and α_k. Pink cells represent the minimum values that are traced back from the last row to the first one using memoization matrix M. The cost function in this thesis is 4D. To simplify illustration, only α is shown in this figure.

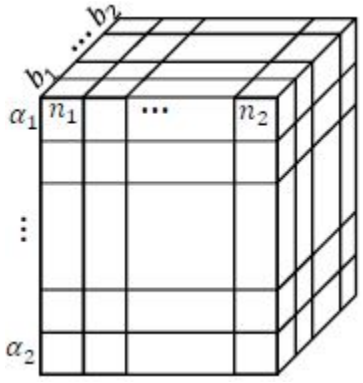

Figure 7: 3D matrix of the cost values at one specific depth. It corresponds to one ROI of the 2D matrix in the Fig. 6 wherein only α was considered as an unknown.

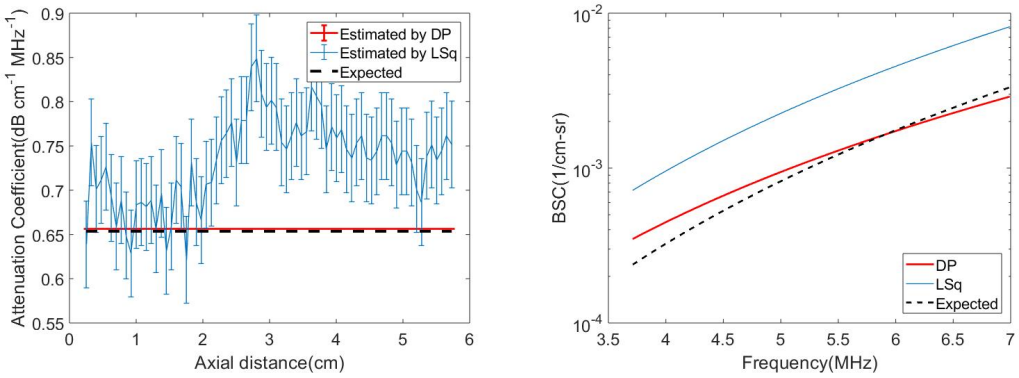

(a) Attenuation Coefficient α (b) Backscatter

Figure 8: LSq and DP estimation in the uniform phantom for (a) attenuation coefficient and (b) backscatter coefficients of Eq. 19.

2.2.3 Data acquisition

Homogeneous phantoms

Two homogeneous tissue-mimicking phantoms, a sample and a reference, were used to compare the performance of the LSq and DP algorithms. The reference phantom consisted of an agarose-based gel with graphite powder within a $15\times15\times5$ cm^3 acrylic box [46]. The sample phantom was a mixture of water-based agarose-propylene glycol and filtered milk within a $16\times10\times10$ cm^3 acrylic box [46]. Both phantoms had scanning windows covered by a 25 μm thick Saran-Wrap (Dow Chemical, Midland MI, USA). Solid glass beads (5-43μm diameter; Spheriglass 3000E, Potter Industries, Malvern, PA) with a mean concentration of 236 scatterers/mm^3 were added to produce incoherent scattering. Ground truth values of each phantom α, b and n (Table 1) were measured from 2.5 cm-thick test samples using narrowband substitution (attenuation) and broadband pulse-echo (backscatter) techniques with single-element transducers [47, 48].

Both phantoms were scanned with a 9L4 38 mm-aperture, linear array transducer on a Siemens Acuson S3000 scanner (Siemens Medical. Solutions USA, Inc., Malvern, PA) operated at 6.6 MHz center frequency and a transmit focal depth of 3 cm. The scanner

Table 1: Ground Truth Values for the Uniform Phantom.

	Reference Phantom	Sample Phantom
α (dB/cm-MHz)	0.670	0.654
b (1/cm-sr-MHz^n)	8.79e-06	1.02e-06
n	3.14	4.16

was enabled with the Axius Direct ultrasound research interface to provide radiofrequency (RF) echo data sampled at 40 MHz [49]. Ten statistically independent RF data frames, each separated by at least one elevational aperture, were acquired from each phantom. The following search ranges were used for both LSq and DP:

$$\alpha_s - 0.5 \leq \alpha \leq \alpha_s + 0.5$$

$$e^{-1} b_s \leq b \leq e^{1} b_s$$

$$n_s - 2 \leq n \leq n_s + 2$$

where α_s, b_s, and n_s are ground truth values of the sample phantom.

Layered phantoms

To compare the performance of the LSq and DP algorithms when estimating piece-wise varying acoustic properties, we applied both methods to RF data from two layered tissue mimicking phantoms, each composed of three axially arranged layers: a 4 cm-thick top layer, a 1.5 cm-thick bottom layer, and a 1.5 cm-thick central layer offering contrast of either attenuation or backscatter with respect to the other two layers [50]. The first phantom had uniform backscatter and higher attenuation in the second layer. The second phantom had uniform attenuation and a central layer with 6 dB higher backscatter than the other two layers. Both phantoms consisted of an emulsion of ultrafiltered milk and water-based

Table 2: Ground Truth Values for Layered Phantom with Uniform Backscatter.

	Layer 1	Layer 2	Layer 3
α (dB/cm-MHz)	0.510	0.779	0.520
b (1/cm-sr-MHz^n)	1.60e-06	3.22e-06	1.60e-06
n	3.52	3.13	3.52

Table 3: Ground Truth Values for Layered Phantom with Uniform Attenuation.

	Layer 1	Layer 2	Layer 3
α (dB/cm-MHz)	0.554	0.580	0.554
b (1/cm-sr-MHz^n)	4.82e-07	3.94e-06	4.82e-07
n	3.80	3.38	3.80

gelatin with 5–43 μm diameter glass beads as sources of scattering (3000E, Potters Industries, Valley Forge, Pennsylvania). Attenuation was controlled by varying amounts of evaporated milk, while the strength of backscatter was increased by augmenting the concentration of glass beads. More detail on the phantom properties can be found in Nam et al [21]. Ground truth values of attenuation and backscatter parameters of the three layers were obtained similarly as for the uniform phantoms and are shown in Tables 2 and 3.

The layered phantoms were scanned with a 18L6 58 mm-aperture, linear array transducer on a Siemens Acuson S2000 scanner (Siemens Medical. Solutions USA, Inc., Malvern, PA) operated at 8.9 MHz center frequency and a transmit focal depth of 5.3 cm. RF echo data from ten statistically independent RF data frames were obtained through the system's Axius Direct ultrasound research interface [49].

Reference echo data were obtained from the top layers of the phantoms by scanning from their flank [21]. The search ranges for both DP and LSq for the three parameters of

interest included the expected values for each phantom's layer:

$$\alpha_{sMin} - 0.5 \leq \alpha \leq \alpha_{sMax} + 0.5$$

$$e^{-1} b_{sMin} \leq b \leq e^{1} b_{sMax}$$

$$n_{sMin} - 2 \leq n \leq n_{sMax} + 2$$

where α_{sMin}, b_{sMin}, and n_{sMin} refer to the minima of the ground truth values in three layers of the layered phantoms for the coefficient α, b, and n, respectively, and α_{sMax}, b_{sMax}, and n_{sMax} correspondingly refer to the maxima of the ground truth values in three layers of the layered phantoms for the coefficient α, b, and n.

2.2.4 Data processing

Both LSq and DP were implemented on the RF data frames using custom-built MATLAB routines. Echo-signal power spectra were computed at different axial and lateral locations by raster-scanning a 4×4 mm^2 spectral estimation window with an 85% overlap ratio and using a multitaper approach with NW=3 [51]. Because different transducers were used in each experiment, this approach produced a power spectrum array with 74 rows and 40 columns for uniform phantoms and 108 rows and 86 columns for layered phantoms, which correspond to different axial and lateral locations, respectively. To reduce correlation between different columns, we selected 4 columns in each phantom separated as far as possible as follows. For the uniform phantom, we selected columns 1, 10, 20 and 40. For the layered phantoms, we picked columns 10, 30, 45, and 80. Each experiment consists of 10 frames, yielding a total of 40 total columns in each experiment. Each cell contained a vector of normalized power spectrum estimates. The LSq and DP estimators were fed with

the normalized power spectra in the frequency range from 3.7–7 MHz corresponding to the spectral band with power content at least 10 dB above the noise floor measured at 15 MHz.

We applied DP and LSq to four different lateral positions from 10 different frames of RF data, i.e 40 sample positions in total. The weights of the regularization term in DP for uniform phantom were set to 10^8 in all 40 sample positions. To provide a fair comparison, we used identical search ranges for both LSq and DP.

In the case of the layered phantoms, the LSq and DP methods were applied to the 108 rows and 40 columns of power spectra from 10 different frames. The weights of the DP regularization were set to $w_\alpha = 10^6$ and $w_b = w_n = 10^3$ for the uniform backscatter phantom, and $w_\alpha = 5 \times 10^6$ and $w_b = w_n = 10$ for the uniform attenuation phantom. These weights are automatically selected as follows. First, we run LSq and investigate the Normalized Range (NR) of b values by dividing the range of LSq estimations for backscatter coefficient b by the mean value of estimates. If the NR is greater than eight, we use the lower regularization value for w_b and w_n above. Otherwise, these weights are set to a higher value as for the uniform backscatter phantom. This is similar to our previous work on Conditional Random Fields (CRF) [52] where we adjust the regularization term based on the data term.

2.3 Results

2.3.1 Uniform Phantom

Fig. 8(a) shows the DP (red) and the LSq (blue) estimates of α_s vs axial distance. Thick, colored lines and errorbars correspond to the mean and standard deviations among 40 estimates at each depth, respectively. Fig. 8(b) show the reconstructed BSC parameters b_s and n_s. Black dashed lines indicates expected values. DP substantially outperforms LSq in

Table 4: The standard deviation (STD) and bias in the Uniform Phantom experiment. The smallest values are highlighted in bold font.

	LSq	DP
Standard Deviation		
α (dB/cm-MHz)	0.049	**2.236e-16**
b (1/cm-sr-MHz^n)	9.402e-07	**1.706e-21**
n	0.410	**3.577e-15**
Bias		
α (dB/cm-MHz)	0.080	**0.003**
b (1/cm-sr-MHz^n)	3.660e-06	**3.341e-06**
n	**0.322**	0.820

estimation of all three parameters.

The bias and standard deviation averaged over the 6cm depth range of α_s, b_s and n_s are shown in Table 4, and the uncertainty in these estimates are shown in Table 5. The units for parameters α and b are respectively dB·cm^{-1}MHz^{-1} and cm^{-1}sr^{-1}MHz^n while parameter n has no units. Both the value of bias and variance, as well as their uncertainty, are substantially lower in DP compared to LSq except for the bias of backscatter coefficient n by LSq which is slightly less than DP; however the uncertainty is still lower for DP.

2.3.2 Layered Phantom

Figs. 9 and 10 show the DP (red) and the LSq (blue) estimates of (a) α_s and (b)-(d) the reconstructed BSC parameters b_s and n_s for each of the three layers vs axial distance. Thick, colored lines and errorbars correspond to the mean and standard deviations among 40 estimates at each depth, respectively. Estimates from the DP method closely follow the depth dependence of effective attenuation α_s, in contrast to the high variance of the LSq method. Black dashed lines indicate expected values. DP substantially outperforms LSq in

Table 5: Uncertainty in STD and Bias in the Uniform Phantom experiment. The smallest values are highlighted in bold font.

	LSq	DP
Standard Deviation		
α (dB/cm-MHz)	0.397	**0.031**
b (1/cm-sr-MHz^n)	6.344e-06	**3.648e-06**
n	2.221	**0.353**
Bias		
α (dB/cm-MHz)	1.744	**0.136**
b (1/cm-sr-MHz^n)	2.790e-05	**1.599e-05**
n	9.767	**1.549**

the estimation of the BSC in each of the three layers.

The standard deviation and bias of the two-layered phantoms, as well as the uncertainties of these measurements, are shown in Tables 6 to 9. Again, DP substantially outperforms LSq in terms of both standard deviations of the estimates as well as the uncertainty in these estimates. Although the bias of LSq and DP estimates are comparable, the uncertainty in the estimated bias is substantially lower in DP.

2.3.3 Effects of expected attenuation

To investigate the performance of DP over a large range of attenuation values, we simulated a new dataset by assigning values of the sample and reference QUS parameters to the log-transformed ratio of power spectra (Eq. 19). Specifically, $0.1 \leq \alpha \leq 2.5$ dB·cm^{-1}MHz^{-1}, and the values of the other parameters were the same as the expected ones for the uniform sample and reference phantoms used in the first experiment. Based on the model developed in Lizzi et al. [53] for the variance of the log-transformed sample-to-reference ratio

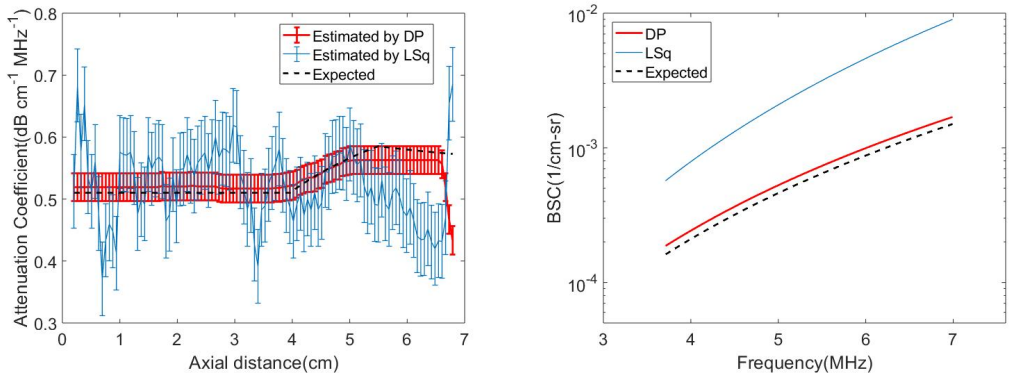

(a) Attenuation Coefficient α

(b) Backscatter Coefficients of Layer 1

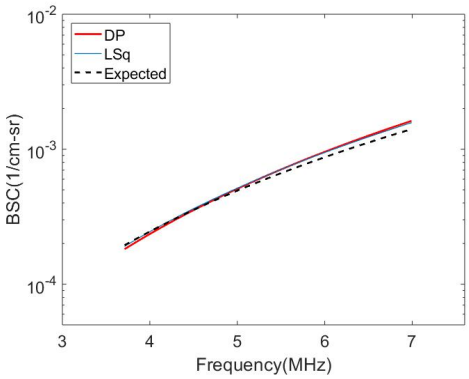

(c) Backscatter Coefficients of Layer 2

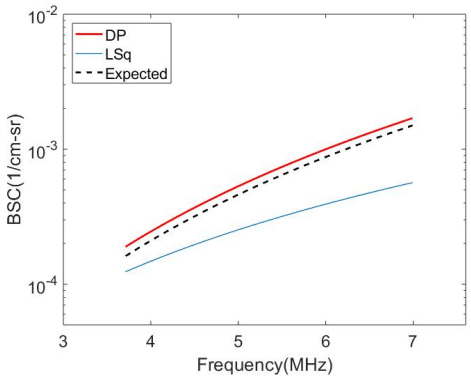

(d) Backscatter Coefficients of Layer 3

Figure 9: LSq and DP estimation of (a) attenuation coefficients and (b–d) backscatter coefficients of Eq. 19 in the three-layered phantom with uniform backscattering coefficients for layer 1, 2, and 3, respectively.

of power spectra, white noise with variance inversely proportional to the number of independent scanlines used to estimate one power spectrum (N=10) was added to the simulated log-transformed normalized power spectra. DP was run on each of the simulated data sets, and we computed the percent bias and standard deviation of the estimated attenuation with respect to the expected values.

The bias and standard deviation in the results of DP and LSq for different attenuation values are plotted in Fig. 11. As it can be observed in Fig. 11(a), for a higher value of the attenuation coefficient, the bias in the estimation of both methods decreases similarly. However, the standard deviation in the estimation of DP in Fig. 11(b) demonstrates the

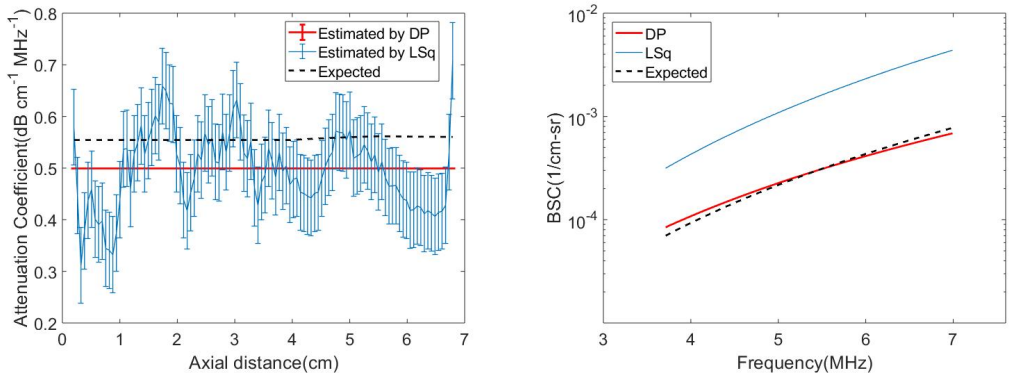

(a) Attenuation Coefficient α

(b) Backscatter Coefficients of Layer 1

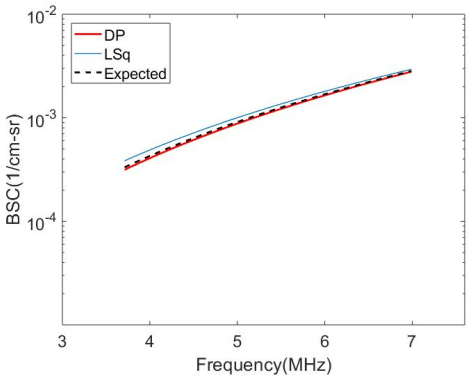

(c) Backscatter Coefficients of Layer 2

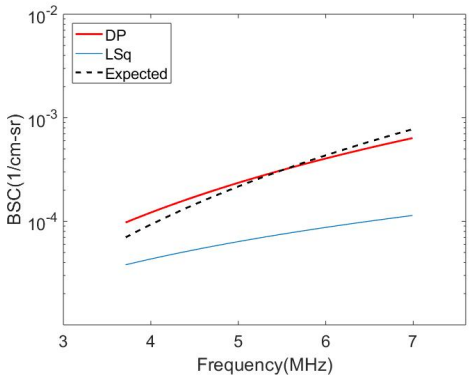

(d) Backscatter Coefficients of Layer 3

Figure 10: LSq and DP estimation of (a) attenuation coefficient and (b–d) backscatter coefficients of Eq. 19 in the three-layered phantom with uniform attenuation coefficients for layer 1, 2, and 3, respectively.

consistency and substantially smaller standard deviation for all values of α compared to LSq. The standard deviation values of DP are multiplied by 10^{12} to be visible in the scale of corresponding values for LSq.

2.3.4 Regularization Weight Analysis

In order to illustrate the impact of regularization weights on the values estimated by DP, we ran the code for a range of regularization weights for the homogeneous phantom to compare the bias (Fig. 12) and standard deviation (Fig. 13) at each weight. The bias and

Table 6: The STD and bias in the Layered Phantom with Uniform Backscatter experiment. In each layer, the smallest values are highlighted in bold font.

	Layer 1		Layer 2		Layer 3	
	LSq	DP	LSq	DP	LSq	DP
STD						
α (dB/cm-MHz)	0.059	**0.001**	0.038	**0.014**	0.069	**0.035**
b (1/cm-sr-MHz^n)	8.423e-07	**7.132e-09**	8.979e-07	**1.697e-08**	5.774e-06	**1.471e-07**
n	0.323	**0.021**	0.400	**0.014**	0.842	**0.081**
Bias						
α (dB/cm-MHz)	0.022	**0.009**	0.028	**0.004**	0.091	**0.028**
b (1/cm-sr-MHz^n)	1.272e-06	**3.441e-07**	**4.155e-07**	1.242e-06	5.527e-06	**5.036e-07**
n	0.117	**0.062**	**0.188**	0.320	0.290	**0.0139**

standard deviation of α, b, and n are shown in Figs. 12 and 13, where the corresponding regularization weight is varied from 1 to 10^{10} while weights of the other two coefficients were fixed at 10^8. These results show that increasing the regularization weight has a small effect on bias while substantially reducing the variance.

2.3.5 DP and LSq Cost Values

In order to observe the functionality of the LSq and DP cost functions at different unknowns along the search ranges, we compared them for the layered phantom with uniform backscatter coefficients in Fig. 8. Again, as it is hard to illustrate the 4D cost function, we set α as the only unknown and calculated the cost function of both LSq and DP at their previously estimated values for b and n and different values of α. Fig. 14 compares the averaged cost function values obtained by running LSq and DP for 40 different RF data of this phantom. In Fig. 15, we added n as the second unknown and plotted the 3D cost function with n and α set as variables. These two figures demonstrate that the DP cost function is more convex (i.e. has a higher second order derivative) and is therefore less susceptible

Table 7: The STD and bias in the Layered Phantom with Uniform Attenuation experiment. In each layer, the smallest values are highlighted in bold font.

	Layer 1		Layer 2		Layer 3	
	LSq	DP	LSq	DP	LSq	DP
STD						
α (dB/cm-MHz)	0.081	**5.037e-16**	0.043	**2.833e-16**	0.067	**2.844e-16**
b (1/cm-sr-MHz^n)	1.123e-06	**3.622e-07**	1.575e-06	**3.336e-07**	5.857e-06	**4.581e-06**
n	0.343	**0.084**	0.508	**0.043**	0.820	**0.212**
Bias						
α (dB/cm-MHz)	**0.050**	0.055	**0.050**	0.059	0.106	**0.061**
b (1/cm-sr-MHz^n)	1.278e-06	**6.677e-07**	**7.073e-07**	8.746e-07	4.521e-06	**3.206e-06**
n	**0.352**	0.458	0.175	**0.083**	1.413	**0.828**

to optimization failures.

2.4 Discussion

The DP method was introduced to simultaneously estimate attenuation and backscatter coefficients of tissue-mimicking phantoms. DP was selected as the optimization technique because it gives the global minimum of the cost function, and is also computationally efficient. The LSq method, which also simultaneously estimates attenuation and backscatter coefficients, was used as a benchmark. Both methods were tested on three phantoms: one homogeneous phantom and two piece-wise homogeneous phantoms.

Fig. 8 clearly indicates that DP results are substantially more precise than LSq results for both attenuation and backscatter coefficients. The LSq results have a large estimation variance, compared to very small variance in DP results. This large improvement in the performance is due to the inclusion of the regularization term, which acts as a prior information and eliminates noisy data. It is also due to the optimization scheme, wherein DP

Table 8: Uncertainties in STD and Bias of Layered Phantom with Uniform Backscatter. In each layer, the smallest values are highlighted in bold font.

	Layer 1		Layer 2		Layer 3	
	LSq	DP	LSq	DP	LSq	DP
STD						
α (dB/cm-MHz)	0.750	**0.067**	0.307	**0.054**	0.264	**0.086**
b (1/cm-sr-MHz^n)	7.170e-06	**1.518e-06**	8.701e-06	**1.685e-06**	1.479e-05	**2.259e-06**
n	3.095	**0.454**	3.385	**0.490**	3.252	**0.588**
Bias						
α (dB/cm-MHz)	3.018	**0.269**	0.783	**0.137**	0.616	**0.199**
b (1/cm-sr-MHz^n)	2.877e-05	**6.102e-06**	2.214e-05	**4.286e-06**	3.429e-05	**5.251e-06**
n	12.457	**1.826**	8.630	**1.249**	7.585	**1.370**

provides the global minimum of the cost function. Moreover, the bias of DP results in the homogeneous phantom is lower than that of LSq. The exception was the bias of n, which was larger for DP. This bias would affect the bias and precision of estimates of the effective scatterer size, a parameter derived from the frequency dependence of backscatter. We are currently investigating the severity of these effects.

Fig. 9 shows the comparison of the performance of DP and LSq for the layered phantom with variable attenuation and constant BSC coefficients. Again, as expected, DP estimates have much smaller variance compared to LSq results. We also see that despite the regularization term, DP estimates reproduce more accurately the depth dependence of the three parameters. This is because the penalty for not following the data term at discontinuities overcomes smoothness penalties.

The last experiment which was on the inhomogeneous phantom with constant attenuation and variable BSC coefficients offered interesting results by both LSq and DP (Fig. 10). Although bias averaged over depth was similar between LSq and DP, LSq showed an unexpected trend of decreasing α_s over depth. In addition, the DP results in (b) to (d), demonstrate that BSC parameters estimated by DP are closer to the expected than those estimated

Table 9: Uncertainties in STD and Bias of Layered Phantom with Uniform Attenuation. In each layer, the smallest values are highlighted in bold font.

	Layer 1		Layer 2		Layer 3	
	LSq	DP	LSq	DP	LSq	DP
STD						
α (dB/cm-MHz)	0.670	**0.156**	0.314	**0.156**	0.237	**0.156**
b (1/cm-sr-MHz^n)	5.006e-06	**1.549e-06**	1.081e-05	**4.788e-06**	1.466e-05	**1.150e-05**
n	3.063	**1.056**	3.503	**1.890**	2.883	**2.206**
Bias						
α (dB/cm-MHz)	2.697	**0.627**	0.800	**0.398**	0.551	**0.365**
b (1/cm-sr-MHz^n)	1.976e-05	**6.208e-06**	2.752e-05	**1.220e-05**	3.368e-05	**2.624e-05**
n	12.326	**4.245**	8.929	**4.817**	6.713	**5.147**

by LSq.

The results of Tables 4 to 9 show the standard deviation and bias of LSq and DP, as well as the uncertainty in these measurements. As expected, DP substantially outperforms LSq in terms of standard deviation of the estimation while giving similar bias. Furthermore, the uncertainty in both standard deviation and bias is substantially lower in the proposed DP method.

Fig. 12 and Fig. 13 show that DP regularization weights have a generally moderate effect on bias and large effect on standard deviation as expected. These weights are often treated as hyperparameters in the machine learning community and have to be adjusted in different applications. Given that ultrasound machines have different imaging presets for imaging different organs (e.g. breast, thyroid, etc.), these hyperparameters can be stored alongside those imaging presets.

As demonstrated by the results, the advantage of the DP method relies on its ability to improve the precision of QUS parameters. In this manuscript, the QUS parameters came from a power-law model of the backscatter coefficient. We chose this model for two

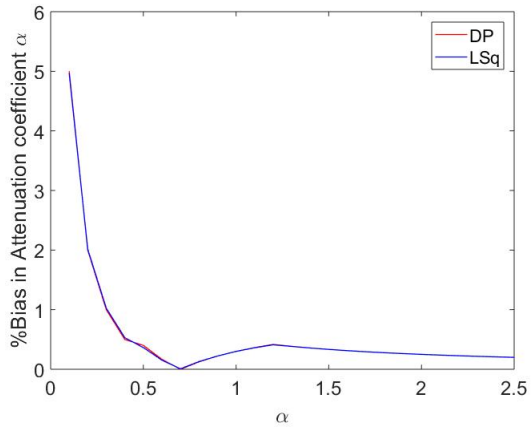

(a) %Bias in Attenuation Coefficient α

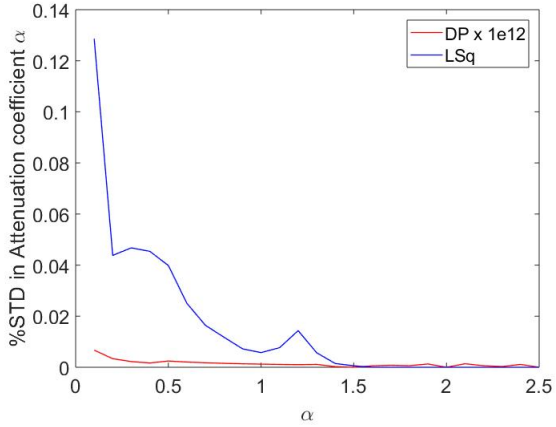

(b) %STD in Attenuation Coefficient α

Figure 11: Percentage of bias and standard deviation in DP and LSq estimations for simulated data with different attenuation coefficients α.

reasons. First, this model was assumed in the LSq method, thus facilitating the comparison. Second, the power law does not assume a physical model for the distribution and size of scatterers in the medium. However, Eq. 19 can be considered a particular case of the more general equation:

$$B(f) = B_0 G(f) \tag{16}$$

where B_0 and $G(f)$ describe the magnitude and frequency dependence of the backscatter coefficient of tissue, respectively. By properly defining $G(f)$, the DP algorithm can be

adapted to quantify different scattering parameters of tissue. For example, $G(f)$ can be defined in terms of scattering form factors to simultaneously estimate attenuation and the effective size of scatterers in tissue, as initially proposed by Bigelow et al. [54]. Under conditions of randomly distributed weak scatters, i.e., diffuse scattering, $G(f)$ takes the form

$$G(f) = f^4 F(f; a_{eff}) \tag{17}$$

where $F(f; a_{eff})$ is the scattering form factor equal to the Fourier transform of the autocovariance function of the scattering field. Under conditions of diffuse scattering, $F(f; a_{eff})$ depends only on the effective scatterer size a_{eff} [55]. Thus, by parameterizing $F(f; a_{eff})$, in terms of a mathematical model, such as a Gaussian function or an exponential function, the DP algorithm can be modified to estimate the effective scatter size, as well as parameters related to the magnitude of scattering and the total attenuation. In this sense, this adaptation of the DP algorithm would expand the work of Bigelow et al. [54, 56] by quantifying the backscatter coefficient magnitude (related to the number density and impedance difference of scatterers – relative to the background) and by using regularization and dynamic programing to improve the precision of the estimated parameters. Alternatively, the DP algorithm can be adapted to compute the packing factor and size of aggregates of Rayleigh scatterers, as proposed by Franceschini et al. [57, 58]. In this case, $G(z, f)$ is defined as the product of the Rayleigh backscatter coefficient for individual scatterers (with f^4 dependence) and the structure factor $S(f)$ which takes into account the interaction of scattering sources. Therefore, the DP strategy can be potentially adapted to quantify parameters from different scattering conditions, improving the precision over previously proposed methods.

We have picked a very large search range to demonstrate that DP provides the correct solution even when no good approximate value is known. When applied to real tissue, based on prior knowledge of the expected values, we can use smaller search ranges that correspond to that tissue, similar to gain settings in imaging presets that current ultrasound

machines have for imaging different organs. Since DP running time depends on the search range, this can substantially reduce the computational complexity of DP. For example, if we halve the search range for α, b and n, the running time reduces from 17 hours to 8 hours. Substantially faster runtime can be achieved by implementing the code in C++, parallel implementation of the method, and multi-resolution search [42].

With a look at all results, it is clear that the regularization term substantially reduces the estimation variance as expected. However, the reduction in estimation bias is not as significant as the reduction in variance. This is also expected from the cost function, as the expected value of the parameters slightly changes with the introduction of the regularization term. Bias-variance trade-off is an important issue in estimation theory and an active field of research [59, 60]. We will investigate this trade-off in future work. We are also investigating the performance of the DP algorithm in the presence of specular reflectors that introduce coherent scattering and, therefore, violate the assumption of diffuse scattering behind the derivation of Eq. 21. In addition, we are exploring situations wherein the frequency dependence of scattering is substantially different between reference and sample due to scatterers of different sizes. Moreover, experiments on phantoms with spherical inclusions are a subject of future work.

2.5 Conclusions

We presented a novel framework for estimation of backscatter quantitative ultrasound parameters based on Dynamic Programming (DP). The new technique incorporates the prior information of depth-continuity of parameters into a cost function that is solved globally using DP. Intuitively, DP considers the data at all depths to estimate $\mathbf{u}$, and finds $\mathbf{u}$ that gives the global minimum of the cost function. All values of $\mathbf{u}$ at different depths are

optimized together in DP, whereas LSq considers each location independently. This substantially reduced the bias and variance in DP estimates compared to LSq in homogeneous phantom.

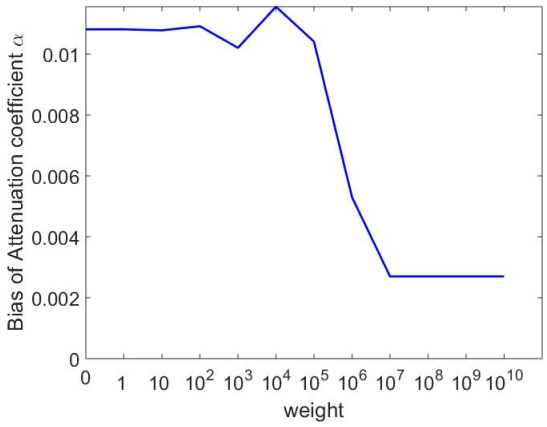

(a) Bias of α in different regularization weights

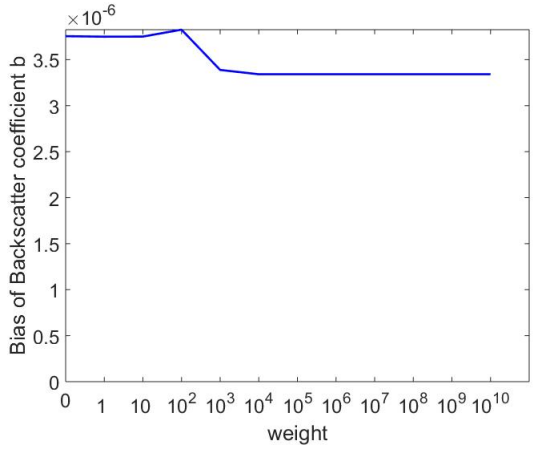

(b) Bias of b in different regularization weights

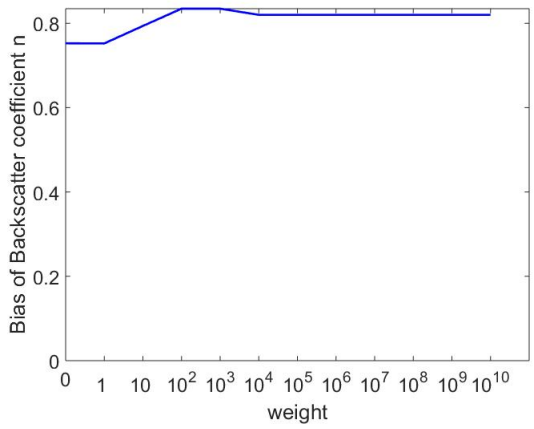

(c) Bias of n in different regularization weights

Figure 12: Bias of DP estimations for coefficients α, b, and n at different weight values used in DP. In (a), the regularization weight for b and n are fixed at 1e8 while it varies for α. In (b), the regularization weight for α and n are fixed at 1e8 while it varies for b. In (c), the regularization weight for α and b are fixed at 1e8 while it varies for n.

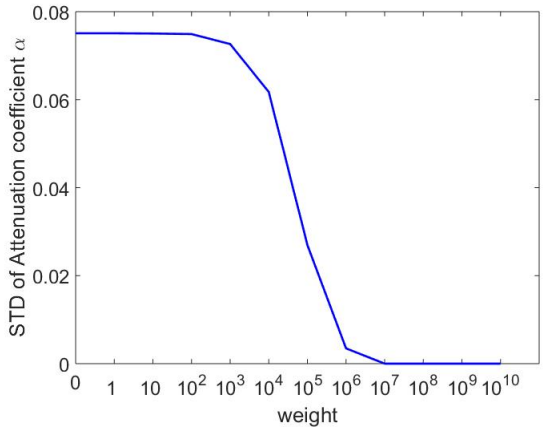

(a) STD of α in different regularization weights

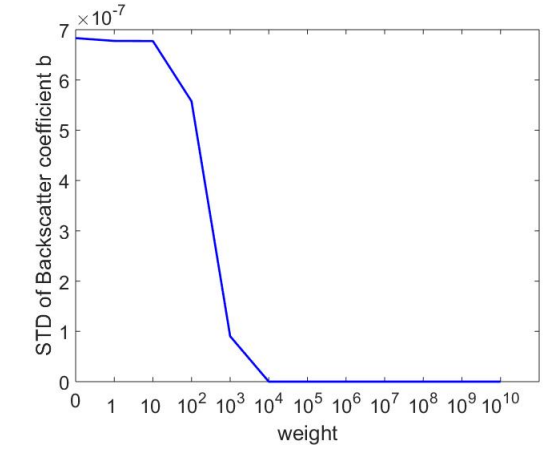

(b) STD of b in different regularization weights

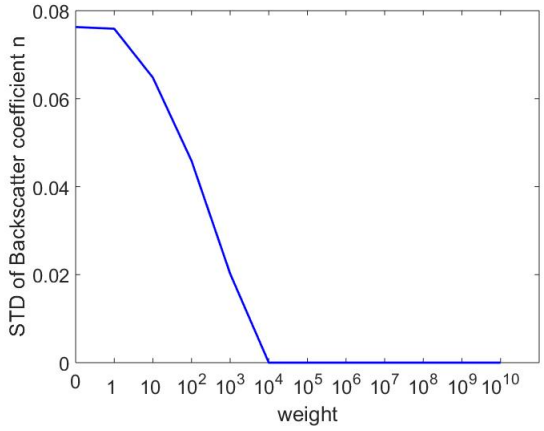

(c) STD of n in different regularization weights

Figure 13: STD of DP estimations for coefficients α, b, and n at different weight values used in DP. In (a), the regularization weight for b and n are fixed at 1e8 while it varies for α. In (b), the regularization weight for α and n are fixed at 1e8 while it varies for b. In (c), the regularization weight for α and b are fixed at 1e8 while it varies for n.

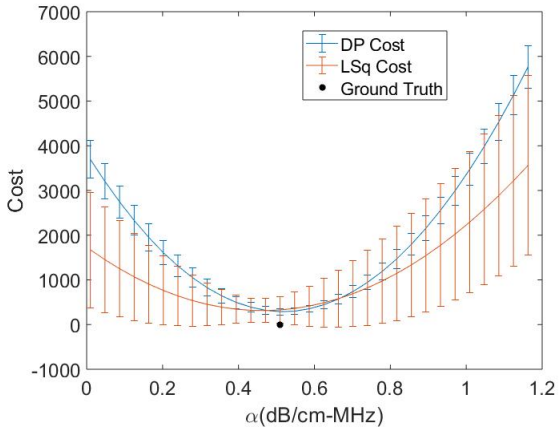

(a) Cost values at different α in Layer 1

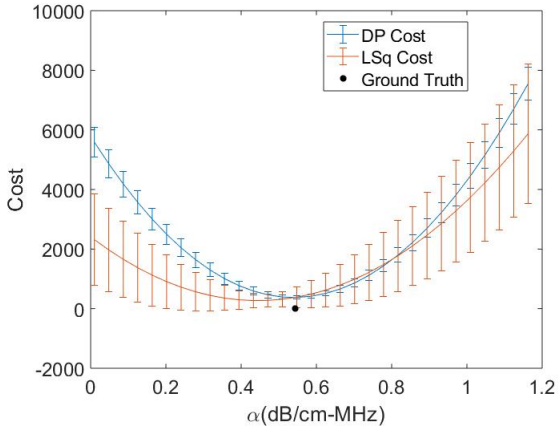

(b) Cost values at different α in Layer 2

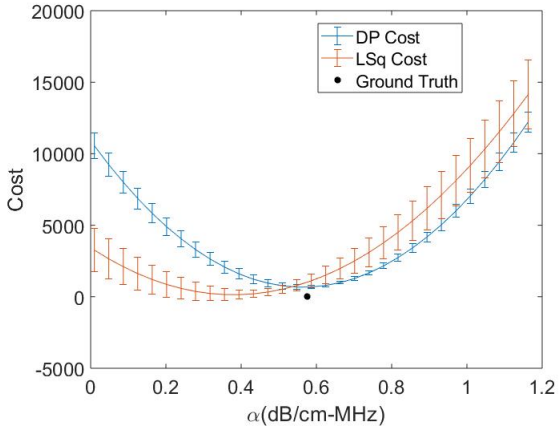

(c) Cost values at different α in Layer 3

Figure 14: Cost values of DP and LSq at different values of α within the search range in each layer of the phantom with uniform backscattering properties. (a) Layer 1 at the depth of 3.5 cm, (b) Layer 2 at the depth of 4.5 cm, (c) Layer 3 at the depth of 6.5 cm.

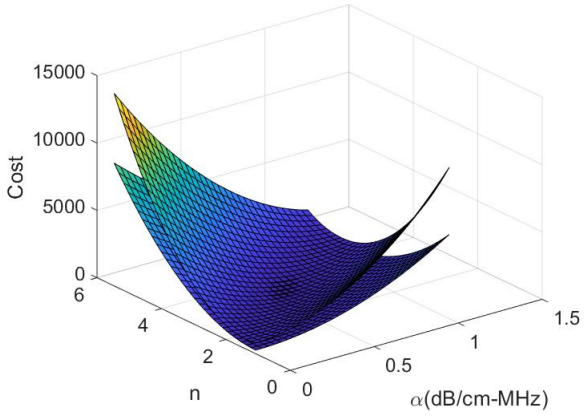

(a) Cost values at different α and n in Layer 1

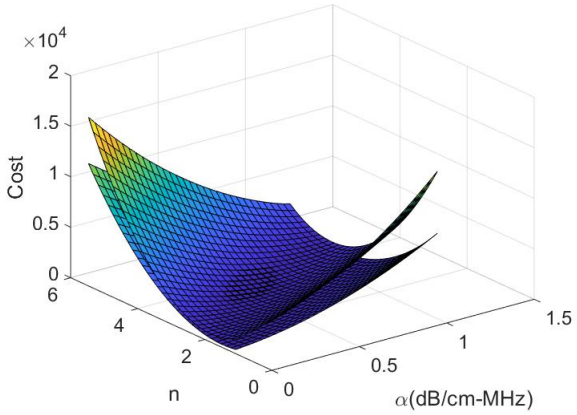

(b) Cost values at different α and n in Layer 2

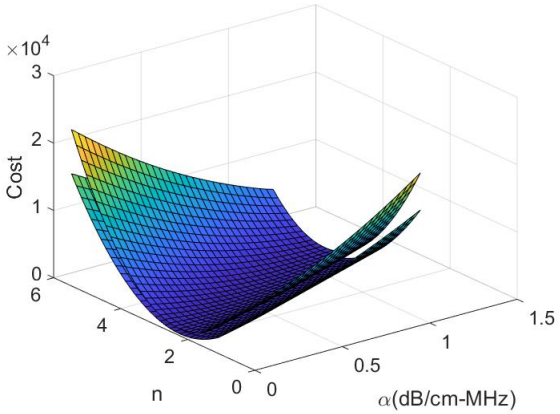

(c) Cost values at different α and n in Layer 3

Figure 15: Cost values of DP and LSq at different values of α and n in each layer of the phantom with uniform backscattering properties. In all three layers, the upper surface is the result by DP. (a) Layer 1 at the depth of 3.5 cm, (b) Layer 2 at the depth of 4.5 cm, (c) Layer 3 at the depth of 6.5 cm.

Chapter 3

L1 and L2 Norm Depth-Regularized Estimation of the Acoustic Attenuation and Backscatter Coefficients Using Dynamic Programming

This chapter has been submitted as a conference paper to the IEEE International Symposium on Biomedical Imaging (ISBI), 2019, and is currently under review.

3.1 Introduction

Despite the information-rich frequency content of these radiofrequency (RF) echo signals, the conventional utilization of ultrasound is a grayscale image, titled B-mode image, which is exclusively the envelope of the amplitude of the ultrasound wave. The QUS methods proposed in the previous chapter provide estimates of attenuation and backscattering properties of the tissue by processing the raw RF signals. Identifying such quantitative acoustic

properties of tissue is of paramount importance in classification of pathology.

Characterization and classification of thyroid nodules [61] and kidneys [62], diagnosis of fatty liver [63], and detection of preterm birth risk [64] are a few of many clinical applications of QUS. However, accurately estimating QUS coefficients is still the challenge of many studies such as [65] and [40]. In order to address this issue, we proposed a Dynamic Programming (DP) algorithm in the previous chapter which is based on a Least Squares (LSq) method with L2 norm depth-regularization assuming piece-wise continuous tissue properties. This novel method substantially reduced the bias and variance of estimation compared to previous work with LSq [21]. Nevertheless, the accuracy of the predicted values at the discontinuities of acoustic properties in inhomogeneous tissues could still be improved.

Here we build upon previous chapter in two ways. First, we propose L1 norm regularization instead of L2 norm for DP optimization to improve parameter estimate accuracy at tissue boundaries. Second, we estimate backscattering and attenuation coefficients of a tissue-mimicking phantom with marked difference in the frequency dependence of backscatter, which is related to the size of diffuse scatterers contributing to the ultrasound echo signal.

3.2 Methods

Quantitative ultrasound often aims at estimating attenuation and backscattering, and parameters derived from them. The total attenuation along an RF line is usually modeled as:

$$A(f, z) = exp(-4\alpha f z) \tag{18}$$

where A is the total attenuation corresponding to frequency f and depth z, and α is the effective attenuation coefficient versus frequency (i.e., the average attenuation from intervening tissues). Backscattering is often parameterized with the following power-law equation:

$$B(f) = bf^n \tag{19}$$

where b is a constant coefficient and n represents the frequency dependence. Our goal is to find the values of α, b and n from Eq. 18 and 19.

Let $S_s(f,z)$ and $S_r(f,z)$ be, respectively, the echo signal power spectra from the sample and reference phantoms obtained using the same ultrasound transducer and the same imaging settings (i.e. frequency, focal properties, etc). Taking the ratio of the two spectra eliminates any dependence on the imaging setting, leaving only attenuation and backscatter-dependent terms:

$$\begin{aligned} RS(f,z) = \frac{S_s(f,z)}{S_r(f,z)} = \frac{B_s(f)}{B_r(f)}.\frac{A_s(f,z)}{A_r(f,z)} = \\ \frac{b_s f^{n_s}}{b_r f^{n_r}} exp\{-4(\alpha_s - \alpha_r)f.z\} \end{aligned} \tag{20}$$

where the subscripts s and r refer to the sample and the reference phantoms, respectively. After taking the natural logarithm and some manipulation, we have:

$$X(f,z) = b + n\ln f - 4\alpha f z \tag{21}$$

where X is the natural logarithm of RS which is known from the experimental data, $b = \ln(b_s/b_r)$, $n = n_s - n_r$, and $\alpha = \alpha_s - \alpha_r$. The goal is to estimate α, b and n, which reveal quantitative properties of the sample. We now show how these parameters can be estimated using DP.

3.2.1 Dynamic Programming (DP)

We proposed DP [22] to solve for α, b and n using the following cost function:

$$C = D + wR \tag{22}$$

where D, w, and R were respectively the data term, regularization wights, and regularization term. The data term was defined as a least squares cost function based on Eq. (21) as:

$$D = \sum_{i=1}^{K} (X(f_i, z) - b - n \ln f_i + 4\alpha f_i z)^2 \tag{23}$$

The regularization weights was defined as:

$$w = [w_\alpha, w_b, w_n] \tag{24}$$

while R was set to L2 norm regularization:

$$R = (\alpha_j - \alpha_{j-1})^2 + (b_j - b_{j-1})^2 + (n_j - n_{j-1})^2 \tag{25}$$

with subscripts j and $j-1$ referring to axial positions at the current and previous rows, and w_α, w_b, and w_n are the regularization weights for each unknown. The Least Squares (LSq) proposed by [21] considered only the minimization of eq. 23.

In this work, we propose to use the L1 norm as follows:

$$R = |\alpha_j - \alpha_{j-1}| + |b_j - b_{j-1}| + |n_j - n_{j-1}| \tag{26}$$

Let $\mathbf{u}$ encapsulates the unknowns as follows:

$$\mathbf{u} = [\alpha, b, n] \tag{27}$$

To find the global optimum of this cost function, we use the efficient DP framework, and formulate the following recursive cost function:

$$C(j, \mathbf{u}_j) = \min_{\mathbf{u}} \{C(j-1, \mathbf{u}_{j-1}) + wR(\mathbf{u}_{j-1}, \mathbf{u})\} + D \tag{28}$$

The minimization is performed on three unknowns $\mathbf{u}$ at each location. The term $C(j-1, \mathbf{u}_{j-1})$ indicates that we need to take into account value of the cost functions from the previous axial row. So, in order to find the $C(j, \mathbf{u}_j)$ value at the current axial position, we have to evaluate R at α, b, and n and add it to the C matrix of the previous axial row. Then, we must find the minimum value of this summation, add the data value D to it, and finally store it in the corresponding element of the cost function matrix.

In the process of finding the minimum value, we also have to store the values of $\mathbf{u}_j$ for which this minimization occurs (technically known as memoization). These locations are stored in M, a 4D matrix with the same size as C.

The DP cost function must be calculated for every axial row. After that, starting from the last axial row, we trace back the minimum points to the first row using the memoization matrix M.

3.3 Data acquisition

Three pairs of tissue mimicking phantoms, each pair including a sample and a reference, were used to compare the performance of LSq, DP L1 and DP L2. The first pair consisted of homogeneous blocks of agarose-based gels. The sample and reference contained 75–90 μm diameter and 5–40 μm diameter glass beads, respectively, creating backscatter coefficients with different frequency dependence. The sample of the second pair was composed of three layers of an emulsion of ultrafiltered milk and water-based gelatin with 5–43 μm diameter glass beads as sources of scattering (3000E, Potters Industries, Valley Forge, Pennsylvania), where the central layer was more attenuating than the outer two. Finally the last sample had three layers of uniform attenuation in which the central layer was of 6 dB higher backscatter than the other two layers. The reference of two layered phantoms was the top layer of each scanned from its side. All phantoms were scanned with a Siemens Acuson S2000 using

linear array transducers as described in [22].

Both LSq and DP were implemented on the RF data frames using custom-built MATLAB routines. Echo-signal power spectra were computed at different axial and lateral locations by raster-scanning a 4×4mm^2 spectral estimation window with a 85% overlap ratio and using a multitaper approach with NW=3 [51]. This approach produced a power spectrum array with 74 rows and 40 columns for the homogeneous phantom and an array with 108 rows and 86 columns for the layered phantoms, which correspond to different axial and lateral locations, respectively. Each cell contained a vector of normalized power spectrum estimates. The LSq and DP estimators were fed with the normalized power spectra in the frequency range from 3.7 MHz to 7 MHz corresponding to the spectral band with power content at least 10dB above the noise floor measured at 15MHz.

We applied L1 and L2 norm DP, as well as LSq to four different lateral positions from 10 different frames of RF data, i.e 40 sample positions in total for each phantom. The weight of the regularization term in DP was set to a fixed value given in Table 10 in all 40 sample positions of the homogeneous phantom (UniformPh), the layered phantom with uniform backscatter coefficients (UniformBSC) and the layered phantom with uniform attenuation (UniformAtt). The following search ranges were used for both LSq and DP:

$$\alpha_{sMin} - 0.5 \leq \alpha \leq \alpha_{sMax} + 0.5$$

$$10^{-1} b_{sMin} \leq b \leq 10^{1} b_{sMax}$$

$$n_{sMin} - 2 \leq n \leq n_{sMax} + 2$$

where α_{sMin}, b_{sMin}, and n_{sMin} refer to the minima of the ground truth values in three layers of the layered phantoms and the ground truth values for the homogeneous phantoms for the coefficient α, b, and n, respectively, and α_{sMax}, b_{sMax}, and n_{sMax} correspondingly refer to the maxima of the ground truth values in three layers of the layered phantoms for the coefficient α, b, and n.

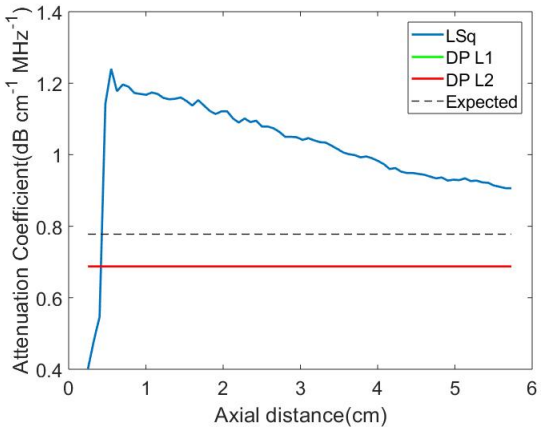

(a) Attenuation Coefficient α of homogeneous phantom 1

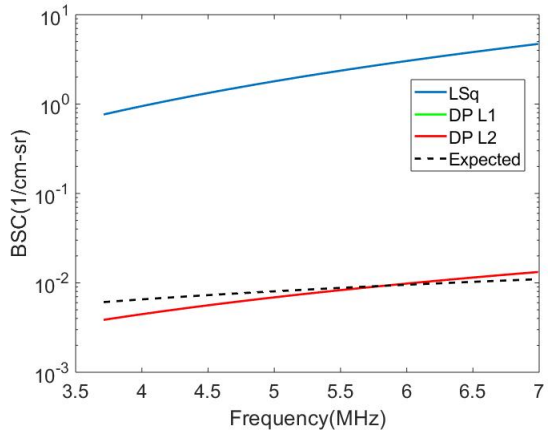

(b) Backscatter Coefficients of homogeneous phantom 1

Figure 16: LSq, DP L1 and DP L2 estimation of (a) attenuation coefficient and (b) backscatter coefficients of Eq. 19 in the homogeneous phantom with large scatterers.

3.4 Results

Figs. 16-18(a) show the DP L1 (green), DP L2 (red) and the LSq (blue) estimates of attenuation vs axial distance for the homogeneous sample of large scatterers, the layered phantom with constant backscatter, and the layered phantom with constant attenuation, respectively. Fig.16 (b) and Figs. 17 and 18 (b)–(d) show the reconstructed sample BSC from estimates of parameters b_s and n_s. Black dashed lines indicates expected values. DP L1 and L2 substantially outperforms LSq in estimation of all three parameters. In Fig.16,

Table 10: The DP regularization weights for each variable

	DP L1			DP L2		
	w_α	w_b	w_n	w_α	w_b	w_n
UniformPh	10^8	10^8	10^8	10^8	10^8	10^8
UniformBSC	10^3	100	100	10^6	10^3	10^3
UniformAtt	10^8	10	10	10^8	10	10

the DP L2 (red) collapsed on DP L1 (green) plot as both regularization norms result in same estimations for constant coefficients.

As demonstrated in the figures, DP L1 outperforms DP L2 in terms of reducing bias error in layered phantoms. Except for the bias of estimated value for backscatter coefficient n, other results by DP L1 were improved compared to DP L2 and LSq. Moreover, L1 norm regularization competitively reduces the STD compared to the L2 norm.

3.5 Conclusions

We proposed employing Dynamic Programming (DP) with an L1 norm regularization term to estimate the backscatter and attenuation coefficients of radiofrequency signals obtained from the ultrasound machine. The L1 norm regularization improved the accuracy of the estimation mainly in the discontinuities of the layered phantoms. This substantially reduced the bias in the attenuation estimation of layered phantoms and slightly improved the accuracy of the backscatter estimations. We also applied the algorithm to a uniform phantom with n markedly different from the reference and compared the results of L1 and L2 norm to LSq. Because of the continuity of the coefficients along the phantom, L1 and L2 result in the same estimation which is profoundly more precise than LSq. We are currently testing the performance of both L1 and L2 regularization in DP when there are sources of coherent

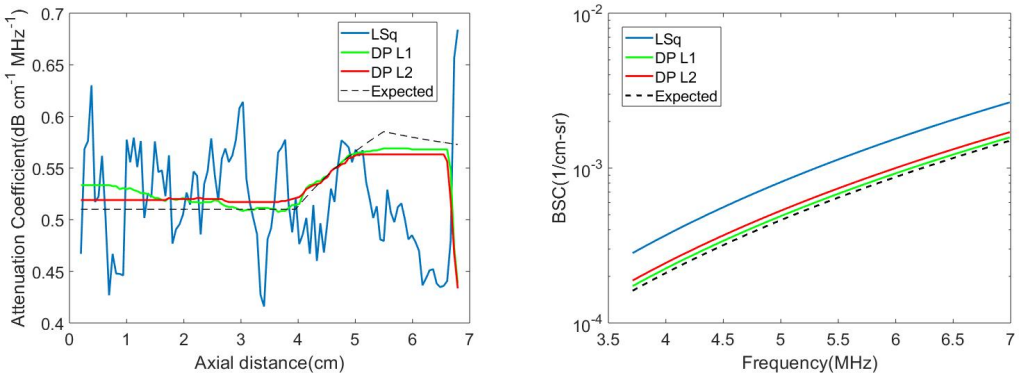

(a) Attenuation Coefficient α

(b) Backscatter Coefficients of Layer 1

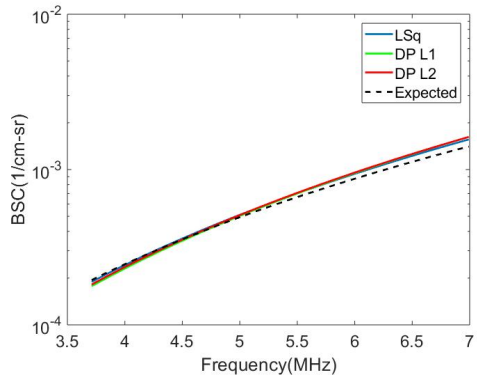

(c) Backscatter Coefficients of Layer 2

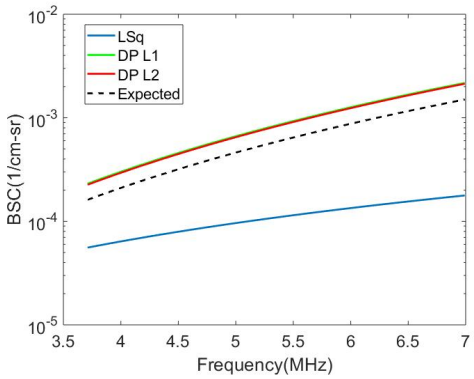

(d) Backscatter Coefficients of Layer 3

Figure 17: LSq, DP L1 and DP L2 estimation of (a) attenuation coefficient and (b–d) backscatter coefficients of Eq. 19 in the three-layered phantom with uniform backscatter coefficients for layer 1, 2, and 3, respectively.

scattering present, such as strong scatterers or specular tissue boundaries.

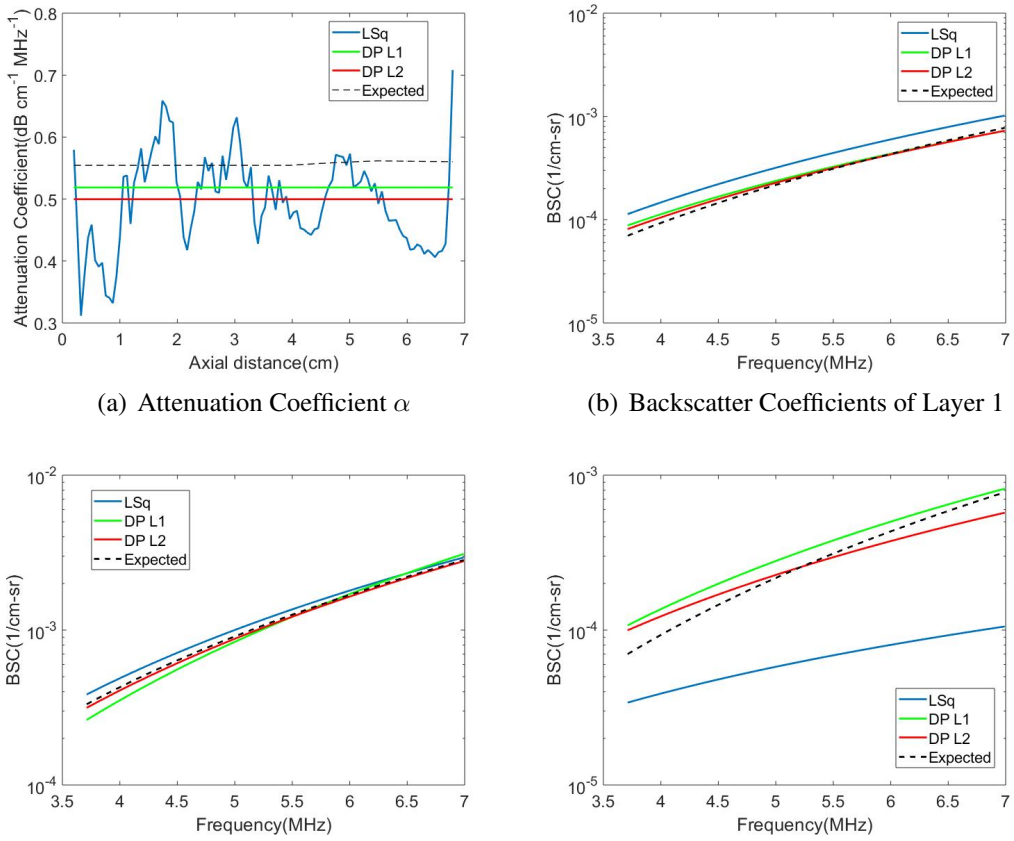

(a) Attenuation Coefficient α

(b) Backscatter Coefficients of Layer 1

(c) Backscatter Coefficients of Layer 2

(d) Backscatter Coefficients of Layer 3

Figure 18: LSq, DP L1 and DP L2 estimation of (a) attenuation coefficient and (b–d) backscatter coefficients of Eq. 19 in the three-layered phantom with uniform attenuation coefficients for layer 1, 2, and 3, respectively.

Chapter 4

Conclusion and Future Work

4.1 Conclusion

Chapter 1 covered the basics of ultrasound imaging with a brief explanation of US physics and beamforming that occur in the US transducer. Further to the B-mode images which is widely used to investigate human body different tissue layers, US echoes could reveal a lot more information about the tissue mechanical characteristics as well as its microstructure properties. Each of these information results in a wide range of studies such as US elastography.

In Chapter 2, we elaborated on Quantitative Ultrasound as extensions of traditional US imaging. QUS investigates the backscattering and attenuation coefficients of US echoes in order to categorize the type of the tissue. Therefore, Chapter 2 started with equations of attenuation and backscattering and explains the parameters and their importance in details. Then a least squares cost function which was previously introduced by Nam et al. [21] is derived and used for comparison to our method.

In this thesis, a Dynamic Programming approach is employed to optimize this cost function. Furthermore, an L2 norm regularization term is also added to the cost function

to incorporate the prior information obtained from the neighboring positions at each depth of the image. The results of this technique represent quite accurate and precise estimations for both backscattering and attenuation coefficients. In addition, regularized DP succeed to reduce the variations in estimations tremendously.

In Chapter 3, an L1 norm regularization term is suggested instead of L2 norm. As expected from an L1 norm regularization component, the estimations of L1 is even more accurate than L2 norm especially in discontinuity points of QUS coefficients. The efficiency of both regularization terms is challenged by applying both to different layered and uniform phantoms. The two cost functions are also applied to a uniform phantom with large scatterers which is conventionally known as a challenging tissue for QUS algorithms. In all cases, DP suggests a highly close estimation of attenuation and backscattering coefficients to the ground truth values.

Dynamic programming globally searches over all possible values of unknowns in the defined search ranges and eventually finds the optimum. Moreover, the regularization term added to the cost function helps with the consistency of estimations in the homogeneous parts of the tissue. Consequently, the algorithm introduced in this thesis outperforms the previous methods profoundly both in terms of reducing bias and standard deviation.

The results of implementing DP with both L1 and L2 norm regularization terms are given at the end of Chapter 2 and Chapter 3. The comparison figures between the estimated values by DP and LSq clearly approves the high performance of DP in terms of bias and variance. Also, the comparisons between L1 and L2 norms imply that L1 norm could track the changes in the coefficients values more accurate than L2 norm.

4.2 Future Work

Quantitative ultrasound has been an active area of research for decades and could be studied in many aspects. Specifically for the method proposed in this thesis, there are numerous ways to improve the accuracy, precision, and robustness of the results as well as reducing the computation burden and make it available for online application. In the following a few of many ideas of the improvement of this method is provided.

Norm 1 regularization term suggested in Chapter 3 could be also applied to the data term of the DP cost function as well as the regularization term. In other words, instead of using the conventional least squares method, the absolute difference of cost value and the expected value is a better suggestion than the least squares in terms of robustness and computation burden reduction. Moreover, an optimization technique such as Gauss-Newton (similar to [9]) can be used to achieve near real-time performance in estimation of the backscatter quantitative ultrasound parameters.

In this thesis, the proposed method was only applied to the data acquired from tissue mimicking phantom. The results of this work were very promising; however, the main challenge of the method is in its application for the data from the in-vivo or ex-vivo tissue.

Recent studies such as [66] and [67] proved many diagnoses and treatment monitoring applications of the backscattering and attenuation as the biomarker features of tissues [68]. Therefore, a great step to move this study forward would be to employ the proposed method for data from a real tissue. Studying a relatively homogenous tissue like liver for cancer diagnosis [69] and a layered tissue such as arms muscles and fat layers for the lymphedema stage monitoring [70, 71] are some of the valuable areas to test this method.

Finally, the method proposed in this thesis has a pre-assumption on the homogeneity of the tissue. However, in real applications, human tissue violates this pre-assumption and the functionality of this method would be affected [72]. One of the methods that is suggested

to overcome inhomogeneity of tissue in microstructure properties investigation is using beam steering. [73] and [74] have shown that beam steering increases the accuracy of the backscattering and attenuation estimations better than the conventional perpendicular beam imaging. Therefore, beam steering could be incorporate with DP to increase the accuracy of the estimations in quantitative ultrasound.

Bibliography

[1] K. A. Kaproth-Joslin, R. Nicola, and V. S. Dogra, "The history of us: from bats and boats to the bedside and beyond: Rsna centennial article," *Radiographics*, vol. 35, pp. 960–970, 2015.

[2] N. J. Hangiandreou, "Physics tutorial for residents: Topics in us," *Imaging & Therapeutic Technology*, vol. 23, pp. 1019–1033, July-August 2003.

[3] J. A. Jensen, "A model for the propagation and scattering of ultrasound in tissue," *The Journal of the Acoustical Society of America*, vol. 89, no. 1, pp. 182–190, 1991.

[4] V. Chan and A. Perlas, "Atlas of ultrasound-guided procedures in interventional pain management," *Springer*, pp. 13–19, 2011.

[5] J. E. Aldrich, "Basic physics of ultrasound imaging," *Critical Care Medicine*, vol. 35, pp. 131–137, May 2007.

[6] P. M. Shankar, V. A. Dumane, J. M. Reid, V. Genis, F. Forsberg, C. W. Piccoli, and B. B. Goldberg, "Classification of ultrasonic b-mode images of breast masses using nakagami distribution," *IEEE Transactions on Ultrasonics, Ferroelectrics, and Frequency Control*, vol. 48, pp. 569–580, March 2001.

[7] G. Heiss, A. R. Sharrett, R. Barnes, L. E. Chambless, M. Szklo, and C. Alzola, "Carotid atherosclerosis measured by b-mode ultrasound in populations: Associations

with cardiovascular risk factors in the aric study," *American Journal of Epidemiology*, vol. 134, pp. 250–256, August 1991.

[8] C. B. Burckhardt, "Speckle in ultrasound b-mode scans," *IEEE Transactions on Sonics and Ultrasonics*, vol. 25, pp. 1–6, Jan 1978.

[9] H. Hashemi and H. Rivaz, "Global time-delay estimation in ultrasound elastography," *IEEE Transactions on Ultrasonics, Ferroelectrics, and Frequency Control*, vol. 64, pp. 1625 – 1636, 2017.

[10] J. e. a. Ophir, "Elastography: Ultrasonic estimation and imaging of the elastic properties of tissues," *Journal of Engineering in Medicine*, vol. 213, pp. 203–233, 1999.

[11] H. Rivaz, E. Boctor, and G. Fichtinger, "A robust meshing and calibration approach for sensorless freehand 3d ultrasound," *Proc. SPIE 6513, Medical Imaging*, 2007.

[12] H. Rivaz, E. Boctor, and G. Fichtinger, "Ultrasound speckle detection using low order moments," *IEEE Ultrasonics Symposium*, pp. 2092–2095, 2006.

[13] A. Lang, P. Mousavi, S. Gill, G. Fichtinger, and P. Abolmaesumi, "Multi-modal registration of speckle-tracked freehand 3d ultrasound to ct in the lumbar spine," *Medical Image Analysis*, pp. 675–686, 2012.

[14] D. Gaitini, Y. Baruch, E. Ghersin, E. Veitsman, H. Kerner, B. Shalem, G. Yaniv, and C. S. H. Azhari, "Feasibility study of ultrasonic fatty liver biopsy: Texture vs. attenuation and backscatter," *Ultrasound in Medicine & Biology*, vol. 30, pp. 1321–1327, October 2004.

[15] H. Tadayyon, A. SadeghiNaini, L. Wirtzfeld, F. C. Wright, and G. Czarnota, "Quantitative ultrasound characterization of locally advanced breast cancer by estimation of its scatterer properties," *Medical Physics*, p. 012903, 2014.

[16] S. C.Lin, E. Heba, T. Wolfson, B. Ang, A. Gamst, A. Han, J. W. Jr, W. D. Jr., M. P.Andre, C. B.Sirlin, and R. Loomba, "Noninvasive diagnosis of nonalcoholic fatty liver disease and quantification of liver fat using a new quantitative ultrasound technique," *Clinical Gastroenterology and Hepatology*, vol. 13, pp. 1337–1345, 2015.

[17] G. I. Baroncelli, "Quantitative ultrasound methods to assess bone mineral status in children: Technical characteristics, performance, and clinical application," *Pediatric Research*, vol. 63, pp. 220–228, March 2008.

[18] C. C. Gler, "Quantitative ultrasound techniques for the assessment of osteoporosis: Expert agreement on current status," *Journal of Bone and Mineral Research*, vol. 12, no. 8, pp. 1280–1288, 1997.

[19] D. C. Bauer, C. C. Gler, and J. A. C. et al, "Broadband ultrasound attenuation predicts fractures strongly and independently of densitometry in older women," *Arch Intern Med*, vol. 157, pp. 629–634, March 1997.

[20] P. F. Felzenszwalb and R. Zabih, "Dynamic programming and graph algorithms in computer vision," *IEEE Transactions on Pattern Analysis and Machine Intelligence*, vol. 33, pp. 721–740, April 2011.

[21] K. Nam, J. A. Zagzebski, and T. J. Hall, "Simultaneous backscatter and attenuation estimation using a least squares method with constraints," *Ultrasound in medicine & biology*, vol. 37, no. 12, pp. 2096–2104, 2011.

[22] Z. Vajihi, I. Mendez, T. Hall, and H. Rivaz, "L1 and l2 norm depth-regularized estimation of the acoustic attenuation and backscatter coefficients using dynamic programming," *Conference proceedings*, Submitted.

[23] E. J. Feleppa, J. Machi, T. Noritomi, T. Tateishi, R. Oishi, E. Yanagihara, and J. Jucha, "Differentiation of metastatic from benign lymph nodes by spectrum analysis in vitro.," *Proc IEEE Ultrason Symp*, vol. 2, pp. 1051–0117, 1997.

[24] N. Rubert and T. Varghese, "Scatterer number density considerations in reference phantom-based attenuation estimation," *Ultrasound in Medicine and Biology*, vol. 40, no. 7, pp. 1680–1696, 2014.

[25] J. Rouyer, T. Cueva, A. Portal, T. Yamamoto, and R. Lavarello, "Attenuation coefficient estimation of the healthy human thyroid in vivo," *Physics Procedia*, vol. 70, pp. 1139–1143, 2015.

[26] T. V. Bartolotta, M. Midiri, M. Galia, G. Runza, M. Attard, G. Savoia, R. Lagalla, and A. E. Cardinale, "Qualitative and quantitative evaluation of solitary thyroid nodules with contrast-enhanced ultrasound: initial results," *European Radiology*, vol. 16, pp. 2234–2241, October 2006.

[27] C. C. Anderson, A. Q. Bauer, M. R. Holland, M. Pakula, P. Laugier, G. L. Bretthorst, and J. G. Miller, "Inverse problems in cancellous bone: Estimation of the ultrasonic properties of fast and slow waves using bayesian probability theory," *The Journal of the Acoustical Society of America*, vol. 128, no. 5, pp. 2940–2948, 2010.

[28] A. M. Nelson, J. J. Hoffman, C. C. Anderson, M. R. Holland, Y. Nagatani, K. Mizuno, M. Matsukawa, and J. G. Miller, "Determining attenuation properties of interfering fast and slow ultrasonic waves in cancellous bone," *The Journal of the Acoustical Society of America*, vol. 130, no. 4, pp. 2233–2240, 2011.

[29] D. Hans and S. Baim, "Quantitative ultrasound (qus) in the management of osteoporosis and assessment of fracture risk," *Journal of Clinical Densitometry*, vol. 20, pp. 322 – 333, 2017.

[30] T. Liu, F. L. Lizzi, R. H. Silverman, and G. J. Kutcher, "Ultrasonic tissue characterization using 2-d spectrum analysis and its application in ocular tumor diagnosis.," *Medical Physics*, vol. 31, pp. 1032–1039, 2004.

[31] R. M. Golub, R. E. Parsons, B. Sigel, E. J. Feleppa, J. Justin, H. A. Zaren, M. Rorke, J. Sokil-Melgar, and H. Kimitsuki, "Differentiation of breast tumors by ultrasonic tissue characterization.," *Ultrasound Med*, vol. 12, pp. 601–608, 1993.

[32] K. Nam, J. A. Zagzebski, and T. J. Hall, "Quantitative assessment of in vivo breast masses using ultrasound attenuation and backscatter," *Ultrasonic imaging*, vol. 35, no. 2, pp. 146–161, 2013.

[33] H. G. Nasief, I. M. Rosado-Mendez, J. A. Zagzebski, and T. J. Hall, "Acoustic properties of breast fat," *Journal of Ultrasound in Medicine*, vol. 34, no. 11, pp. 2007–2016, 2015.

[34] K. Parker, "Scattering and reflection identification in h-scan images," *Physics in Medicine & Biology*, vol. 61, no. 12, p. L20, 2016.

[35] G. Ge, R. Laimes, J. Pinto, J. Guerrero, H. Chavez, C. Salazar, R. J. Lavarello, and K. J. Parker, "H-scan analysis of thyroid lesions," *Journal of Medical Imaging*, vol. 5, no. 1, p. 013505, 2018.

[36] M. F. Insana, T. J. Hall, J. G. Wood, and Z. Y. Yan, "Renal ultrasound using parametric imaging techniques to detect changes in microstructure and function.," *Invest Radiol*, vol. 28, pp. 720–725, 1993.

[37] M. L. Oelze and J. Mamou, "Review of quantitative ultrasound: Envelope statistics and backscatter coefficient imaging and contributions to diagnostic ultrasound,"

IEEE Transactions on Ultrasonics, Ferroelectrics, and Frequency Control, vol. 63, pp. 1373–1377, 2016.

[38] P. Laugier, S. Bernard, Q. Vallet, J.-G. Minonzio, and Q. Grimal, "A review of basic to clinical studies of quantitative ultrasound of cortical bone," *The Journal of the Acoustical Society of America*, vol. 137, no. 4, pp. 2285–2285, 2015.

[39] L. X. Yao, J. A. Zagzebski, and E. L. Madsen, "Backscatter coefficient measurements using a reference phantom to extract depth-dependent instrumentation factors.," *Ultrasound Imaging*, vol. 12, pp. 58–70, 1990.

[40] A. Coila, L. Anders, J. Roberto, and R. Lavarello, "Regularized spectral log difference technique for ultrasonic attenuation imaging," *IEEE transactions on ultrasonics, ferroelectrics, and frequency control*, vol. 65, no. 3, pp. 378–389, 2018.

[41] J. Jiang and T. J. Hall, "A regularized real-time motion tracking algorithm using dynamic programming for ultrasonic strain imaging," *2006 IEEE Ultrasonics Symposium*, pp. 606–609, 2006.

[42] H. Rivaz, E. Boctor, E. Foroughi, R. Zellars, G. Fichtinger, and G. Hager, "Ultrasound elastography: a dynamic programming approach," *IEEE Transactions on Medical Imaging*, vol. 27, pp. 1373–1377, 2008.

[43] Z. Christopher, A. Penate-Sanchez, and M. Pham, "A dynamic programming approach for fast and robust object pose recognition from range images.," *IEEE Conference on Computer Vision and Pattern Recognition (CVPR)*, pp. 196–203, 2015.

[44] K. Nam, I. M. Rosado-Mendez, N. C. Rubert, E. L. Madsen, J. A. Zagzebski, and T. J. Hall, "Ultrasound Attenuation Measurements Using a Reference Phantom with Sound Speed Mismatch," *Ultrasonic Imaging*, vol. 33, pp. 251–263, October 2011.

[45] A. L. Coila and R. Lavarello, "Regularized spectral log difference technique for ultrasonic attenuation imaging," *IEEE transactions on ultrasonics, ferroelectrics, and frequency control*, vol. 65, no. 3, pp. 378–389, 2018.

[46] F. Dong, E. L. Madsen, M. C. MacDonald, and J. A. Zagzebski, "Nonlinearity parameter for tissue-mimicking materials," *Ultrasound in medicine & biology*, vol. 25, no. 5, pp. 831–838, 1999.

[47] E. Madsen, G. Frank, P. Carson, P. Edmonds, L. Frizzell, B. Herman, F. Kremkau, W. O'Brien, K. Parker, and R. Robinson, "Interlaboratory comparison of ultrasonic attenuation and speed measurements.," *Journal of ultrasound in medicine*, vol. 5, no. 10, pp. 569–576, 1986.

[48] J. F. Chen, J. A. Zagzebski, and E. L. Madsen, "Tests of backscatter coefficient measurement using broadband pulses," *IEEE transactions on ultrasonics, ferroelectrics, and frequency control*, vol. 40, no. 5, pp. 603–607, 1993.

[49] S. S. Brunke, M. Insana, J. J. Dahl, C. Hansen, M. Ashfaq, and H. Ermert, "An ultrasound research interface for a clinical system," *IEEE transactions on ultrasonics, ferroelectrics, and frequency control*, vol. 54, no. 1, pp. 198–210, 2007.

[50] K. Nam, I. M. Rosado-Mendez, L. A. Wirtzfeld, G. Ghoshal, A. D. Pawlicki, E. L. Madsen, R. J. Lavarello, M. L. Oelze, J. A. Zagzebski, W. D. OBrien Jr, *et al.*, "Comparison of ultrasound attenuation and backscatter estimates in layered tissue-mimicking phantoms among three clinical scanners," *Ultrasonic imaging*, vol. 34, no. 4, pp. 209–221, 2012.

[51] I. M. Rosado-Mendez, K. Nam, T. J. Hall, and J. A. Zagzebski, "Task-oriented comparison of power spectral density estimation methods for quantifying acoustic attenuation in diagnostic ultrasound using a reference phantom method," *Ultrasonic imaging*, vol. 35, no. 3, pp. 214–234, 2013.

[52] Z. Karimaghaloo, H. Rivaz, D. Arnold, D. Collins, and T. Arbel, "Temporal hierarchical adaptive texture crf for automatic detection of gadolinium-enhancing multiple sclerosis lesions in brain mri," *IEEE Trans. Medical Imaging*, vol. 34, pp. 1227–1241, 2015.

[53] F. L. Lizzi, M. Astor, E. J. Feleppa, M. Shao, and A. Kalisz, "Statistical framework for ultrasonic spectral parameter imaging.," *Ultrasound in Medicine & Biology*, pp. 1371–1382, 1997.

[54] T. A. Bigelow, M. L. Oelze, and W. D. O'Brien, "Estimation of total attenuation and scatterer size from backscattered ultrasound waveforms," *The Journal of the Acoustical Society of America*, pp. 1431–1439, 2005.

[55] M. F. Insana and T. J. Hall, "Characterising the microstructure of random media using ultrasound," *Physics in Medicine and Biology*, vol. 35, no. 10, pp. 1373–1386, 1990.

[56] T. A. Bigelow, M. L. Oelze, and W. D. O'Brien, "Signal processing strategies that improve performance and understanding of the quantitative ultrasound spectral fit algorithm," *The Journal of the Acoustical Society of America*, pp. 1808–1819, 2005.

[57] E. Franceschini, F. T. H. Yu, and G. Cloutier, "Simultaneous estimation of attenuation and structure parameters of aggregated red blood cells from backscatter measurements," *The Journal of the Acoustical Society of America*, no. 123, pp. EL85–EL91, 2008.

[58] E. Franceschini, F. T. H. Yu, and F. Destrempes, "Ultrasound characterization of red blood cell aggregation with intervening attenuating tissue-mimicking phantoms," *The Journal of the Acoustical Society of America*, no. 127, pp. 1104–1115, 2010.

[59] S. Geman, E. Bienenstock, and R. Doursat, "Neural networks and the bias/variance dilemma," *Neural computation*, vol. 4, no. 1, pp. 1–58, 1992.

[60] O. Dekel, R. Eldan, and T. Koren, "Bandit smooth convex optimization: Improving the bias-variance tradeoff," in *Advances in Neural Information Processing Systems*, pp. 2926–2934, 2015.

[61] A. Coila, R. Laimes, C. Salazar, J. Rouyer, G. Jimenez, J. A. Pinto, J. Guerrero, and R. Lavarello, "In vivo attenuation estimation in human thyroid nodules using the regularized spectral log difference technique: Initial pilot study," *IEEE International Ultrasonics Symposium (IUS)*, pp. 1–4, 2017.

[62] K. B. Raja, M. Madheswaran, and K. Thyagarajah, "Ultrasound kidney image analysis for computerized disorder identification and classification using content descriptive power spectral features," *Journal of Medical Systems*, vol. 31, pp. 307–317, 2007.

[63] N. Khov, A. Sharma, and T. R. Riley, "Bedside ultrasound in the diagnosis of nonalcoholic fatty liver disease," *World journal of gastroenterology*, vol. 20, pp. 6821–6826, 2014.

[64] B. L. McFarlin, V. Kumar, T. A. Bigelow, D. G. Simpson, R. C. White-Traut, J. S. Abramowicz, and W. D. O. Jr, "Beyond cervical length: A pilot study of ultrasonic attenuation for early detection of preterm birth risk," *Ultrasound in Medicine & Biology*, vol. 41, pp. 3023–3029, 2015.

[65] A. Coila, G. Torres, J. Rouyer, S. Aristizabal, M. Urban, and R. Lavarello, "Recent developments in spectral-based ultrasonic tissue characterization," *International Symposium on Biomedical Imaging (ISBI)*, pp. 1018–1021, April 2018.

[66] E. Picano and M. Paterni, "Ultrasound tissue characterization of vulnerable atherosclerotic plaque," *International Journal of Molecular Sciences*, vol. 16, pp. 10121–10133, May 2015.

[67] M. Horii, H. Fujiwara, R. Sakai, K. Sawada, Y. Mikami, S. Toyama, E. Ozaki, N. Kuriyama, M. Kurokawa, , and T. Kubo, "New quantitative ultrasound techniques for bone analysis at the distal radius in hip fracture cases: differences between femoral neck and trochanteric fractures," *Clinical cases in mineral and bone metabolism*, vol. 14, pp. 23–27, 2017.

[68] R. M. Vlad, N. M. Alajez, A. Giles, M. C. Kolios, and G. J. Czarnota, "Quantitative ultrasound characterization of cancer radiotherapy effects in vitro," *International Journal of Radiation Oncology, Biology, Physics*, vol. 72, no. 4, pp. 1236 – 1243, 2008.

[69] T. Nguyen, A. Podkowa, R. J. Miller, M. L. Oelze, and M. Do, "In-vivo study of quantitative ultrasound parameters in fatty rabbit livers," *IEEE International Ultrasonics Symposium (IUS)*, pp. 1–4, September 2017.

[70] H. Hashemi, S. Fallone, M. Boily, A. Towers, R. Kilgour, and H. Rivaz, "Assessment of mechanical properties of tissue in breast cancer-related lymphedema using ultrasound elastography," *IEEE Transactions on Ultrasonics, Ferroelectrics, and Frequency Control*, In press.

[71] R. Dinniwell and G. Czarnota, "2091464 quantitative ultrasound methods for lymphedema assessment," *Ultrasound in Medicine & Biology*, vol. 41, no. 4, Supplement, p. S163, 2015.

[72] H. Rivaz, R. Zellars, G. Hager, G. Fichtinger, and E. Boctor, "Beam steering approach for speckle characterization and out-of-plane motion estimation in real tissue," pp. 781–784, Oct 2007.

[73] Q. W. Guerrero, H. Feltovich, I. M. Rosado-Mendez, L. C. Carlson, G. Li, and T. J. Hall, "Anisotropy and spatial heterogeneity in quantitative ultrasound parameters: Relevance to the study of the human cervix," *Ultrasound in Medicine & Biology*, vol. 44, pp. 1493–1503, 2018.

[74] Q. W. Guerrero, I. M. Rosado-Mendez, L. C. Drehfal, H. Feltovich, and T. J. Hall, "Quantifying backscatter anisotropy using the reference phantom method," *IEEE Transactions on Ultrasonics, Ferroelectrics, and Frequency Control*, vol. 64, pp. 1063–1077, July 2017.